

# Climatic factors contributing to long-term variations of fine dust concentration in the United States

Bing Pu<sup>1,2</sup> and Paul Ginoux<sup>2</sup>

<sup>1</sup>Atmospheric and Oceanic Sciences Program, Princeton University,

Princeton, New Jersey 08544

<sup>2</sup>NOAA Geophysical Fluid Dynamics Laboratory, Princeton, New Jersey 08540

10

11

12

13

14

15

16

17

18

19

20

21

22

23

24 **Abstract.** High concentration of dust particles can cause respiratory problems and  
25 increase non-accidental mortality. Studies found fine dust (with aerodynamic diameter  
26 less than 2.5 microns) is an important component of the total PM2.5 mass in the western  
27 and central U.S. in spring and summer and has positive trends. This work examines  
28 factors influencing long-term variations of fine dust concentration in the U.S. using  
29 station data from the Interagency Monitoring Protected Visual Environments  
30 (IMPROVE) network during 1990-2015. The variations of the fine dust concentration can  
31 be largely explained by the variations of precipitation, surface bareness, and 10 m wind  
32 speed. Moreover, including convective parameters such as convective inhibition (CIN)  
33 and convective available potential energy (CAPE) better explains the variations and  
34 trends over the Great Plains from spring to fall.

35 While the positive trend of fine dust concentration in the Southwest in spring is  
36 associated with precipitation deficit, the increasing of fine dust over the central Great  
37 Plains in summer is largely associated with an enhancing of CIN and a weakening of  
38 CAPE, which are related to increased atmospheric stability due to surface drying and  
39 lower troposphere warming. The positive trend of the Great Plains low-level jet also  
40 contributes to the increasing of fine dust concentration in the central Great Plains in  
41 summer via its connections with surface winds and CIN.

42 Summer dusty days in the central Great Plains are usually associated with a  
43 westward extension of the North Atlantic subtropical high that intensifies the Great Plains  
44 low-level jet and also results in a stable atmosphere with subsidence and reduced  
45 precipitation.

46

47      **1. Introduction**

48            Mineral dust is one of the most abundant atmospheric aerosols by mass. It is lifted  
49            to the atmosphere by strong wind from dry and bare surfaces. Severe dust storms have  
50            far-reaching socioeconomic impacts, affecting public transportation and health (e.g.,  
51            Morman and Plumlee, 2013) by degrading visibility, causing traffic accidents, breathing  
52            problems, and lung diseases. Dust storms are found to be associated with increases in  
53            non-accidental mortality in the U.S. during 1993-2005 (Crooks et al., 2016).

54            Major dust sources in the United States are located over the western U.S., where  
55            several deserts are located, e.g., the Mojave, Sonoran, and northern Chihuahuan deserts,  
56            and over the central U.S., where the dust sources are largely anthropogenic, in association  
57            with agriculture activities (Ginoux et al., 2012). Climate models project a drying trend in  
58            the late half of the twenty-first century over the southwest and central U.S. (e.g., Seager  
59            et al., 2007; Cook et al., 2015), regions largely collocated with the major dust sources in  
60            the U.S. This raises questions such as how future dust activities will change in the U.S.  
61            To project future dust variations, we first need to understand how dust activity varies in  
62            the present day. Pu and Ginoux (2017) explored this question using dust optical depth  
63            (DOD) derived from MODIS Deep Blue (M-DB2) aerosol products during 2003-2015  
64            and found that variations of dust activity are largely associated with precipitation, near  
65            surface wind speed, and surface bareness.

66            While DOD describes the total optical depth of dust aerosols with different sizes  
67            and is widely used to study climate-dust interactions, fine dust with aerodynamic  
68            diameter less than  $2.5 \mu\text{m}$  is more frequently used for air quality purposes. The diameter  
69            of dust aerosols usually ranges from 0.1 to  $50 \mu\text{m}$  (Duce, 1995), with measured volume

70 median diameters varying from 2.5 to 9  $\mu\text{m}$  (Reid et al., 2003) and clay (diameter  $< 2 \mu\text{m}$   
71 ) mass fraction representing less than 10% (Kok, 2011). In terms of air quality, fine dust  
72 contributed about 40-50% of total Particulate Matter 2.5 (PM2.5) mass over the  
73 southwestern U.S. in spring and about 20-30% over the southwestern to central U.S. in  
74 summer (Hand et al., 2017).

75 Stations in the network of the Interagency Monitoring of Protected Visual  
76 Environments (IMPROVE) have collected PM2.5 samples in the U.S. since 1988 (Malm  
77 et al., 1994; Hand et al., 2011). Analysis of chemical elements is used to derive fine dust  
78 concentration. Due to its long temporal coverage, this dataset has been widely used to  
79 study long-term variations of fine dust in the U.S. Using IMPROVE data, Hand et al.  
80 (2016) found an increasing trend of fine dust in spring in the southwestern U.S. during  
81 1995-2014 and related this trend to a negative Pacific decadal oscillation (PDO) from  
82 2007 to 2014. Tong et al. (2017) also found a rapid increase of dust storm activity in the  
83 Southwest from 1988 to 2011 and related the trend to sea surface temperature variations  
84 in the Pacific. Later, Hand et al. (2017) examined the trends of IMPROVE fine dust  
85 concentration in different seasons from 2000 to 2014 and found positive trends over the  
86 southwestern U.S. in spring and over the central U.S. in summer and fall. Similarly,  
87 Zhang et al. (2017) also found a positive trend of fine dust over the central U.S. from  
88 2005 to 2015 and suggested this trend may contribute to the increase of absorbing aerosol  
89 optical depth in the region. Nonetheless, the possible causes of the fine dust trends,  
90 especially the increase of fine dust over the central U.S., have not been thoroughly  
91 discussed by previous studies. Here, we explore the underlying factors driving the long-  
92 term variations of fine dust from 1990 to 2015. We start with local environmental factors

93 and then examine the possible influence of the low-level jet over the Great Plains on fine  
94 dust concentration in summer.

95 The following section describes the data and analysis method used in the paper.

96 Section 3 presents our major results and conclusions are summarized in Section 4.

97

## 98 **2. Data and Methodology**

### 99 **2.1 IMPROVE fine dust**

100 IMPROVE stations are located in National Parks and wilderness areas in the  
101 United States, with PM<sub>2.5</sub> sampling performed every third day since March 1988.  
102 Records from 204 stations within a domain of 15°-53°N and 60°-127°W are used in this  
103 study, and most of the stations contain data longer than 10 years (Fig. S1 in the  
104 Supplement). Elemental concentration is determined from X-ray fluorescence, and fine  
105 dust concentration is calculated using the concentrations of aluminum (Al), silicon (Si),  
106 calcium (Ca), iron (Fe), and titanium (Ti) by assuming oxide norms associated with  
107 predominant soil species (Malm et al., 1994; their Eq. 5). More details regarding  
108 IMPROVE stations, sampling, and analysis method can be found in previous studies  
109 (Hand et al., 2011;2012; 2016;2017).

110 We averaged daily station data to monthly means and then interpolated them to a  
111 0.5° by 0.5° grid using inverse distance weighted interpolation, i.e., weights depending  
112 on the inverse cubic distance between the site location and the interpolated grid point. In  
113 daily composite analysis, daily station data are interpolated to a 0.5° by 0.5° grid using  
114 the same method.

115 Following Pu and Ginoux (2017), several dusty regions are selected for analysis.  
116 The southwestern U.S. (WST for short; 32°-42°N, 105°-124°W) and Great Plains (GP for  
117 short; 25°-49°N, 95°-105°W) cover the major dust source regions (black boxes in Fig. 1),  
118 while the central Great Plains (32°-40°N, 95°-102°W) is chosen to examine the  
119 increasing trend of fine dust in the region.

120

## 121 **2.2 Cloud-Aerosol Lidar with Orthogonal Polarization (CALIOP) products**

122 CALIOP is the two-wavelength polarization lidar carried by Cloud-Aerosol Lidar  
123 and Infrared Pathfinder Satellite Observation (CALIPSO) satellite, which was launched  
124 in April 2006 (Winker et al., 2004;2007). CALIOP measures backscattered radiances  
125 attenuated by the presence of aerosols and clouds, whose microphysical and optical  
126 properties are retrieved. Daily products are available since June 2006. To examine the  
127 vertical profile of dust concentration in the U.S., the daily 532 nm total attenuated  
128 backscatter from Level 1 product and depolarization ratio from Level 2 product are used.

129 Depolarization ratio can be used to separate spherical and non-spherical hydrometeors  
130 and aerosols (Sassen, 1991), and here  $\geq 0.2$  is used to separate non-spherical dust from  
131 other aerosols (Li et al., 2010).

132

## 133 **2.2 Precipitation**

134 The Precipitation Reconstruction over Land (PRECL; Chen et al., 2002) from the  
135 National Oceanic and Atmospheric Administration (NOAA) is a global analysis available  
136 monthly from 1948 to present at a 1° by 1° resolution, and is suitable to study long-term  
137 connections between fine dust and precipitation. The dataset is derived from gauge

138 observations from the Global Historical Climatology Network (GHCN), version 2, and  
139 the Climate Anomaly Monitoring System (CAMS) datasets. Monthly precipitation from  
140 1990 to 2015 is used.

141

142 **2.3 Leaf area index (LAI)**

143 Monthly LAI derived from the version 4 of Climate Data Record (CDR) of  
144 Advanced Very High Resolution Radiometer (AVHRR) surface reflectance (Claverie et  
145 al., 2014) and produced by the National Aeronautics and Space Administration (NASA)  
146 Goddard Space Flight Center (GSFC) and the University of Maryland is used. The  
147 gridded monthly data are on a  $0.05^{\circ}$  by  $0.05^{\circ}$  horizontal resolution and available from  
148 1981 to present. This dataset is selected due to its high spatial resolution and long  
149 temporal coverage. Monthly data from 1990 to 2015 are used. A detailed discussion on  
150 the algorithm and evaluation of the dataset can be found by Claverie et al. (2016).

151 Surface bareness is derived from seasonal mean LAI, and is calculated following  
152 Pu and Ginoux (2017),

153 
$$\text{Bareness} = -\exp(LAI) \quad . \quad (1)$$

154

155 **2.4 Reanalysis**

156 North American Regional Reanalysis (NARR; Mesinger et al., 2006) provides 3-  
157 hourly, daily, and monthly meteorological variables from 1979 to the present at a high  
158 spatial resolution (i.e., about 32km horizontally). Precipitation in the NARR is  
159 assimilated with observations. The reanalysis reasonably captures the hydroclimatic  
160 fields in the continental U.S. on multiple time scales (Ruiz-Barradas and Nigam, 2006;

161 Ruane, 2010a, b), thus is suitable to study the connection between fine dust concentration  
162 and local hydroclimatic variables. Here daily and monthly convective variables such as  
163 convective inhibition (CIN), and convective available potential energy (CAPE) are used.  
164 CIN is defined as the energy that a parcel needs to overcome to rise above the level of  
165 free convection (LFC), and is usually written as:

$$166 \quad CIN = - \int_{P_{sfc}}^{P_{LFC}} R_d (T_{vp} - T_{ve}) dlnp \quad , \quad (2)$$

167 where  $P_{LFC}$  is the pressure at LFC,  $P_{sfc}$  is the pressure at the surface,  $R_d$  is the specific gas  
168 constant for dry air,  $T_{vp}$  is the virtual temperature of the lifted parcel, and  $T_{ve}$  is the virtual  
169 temperature of the environment. ~~By definition~~, CIN is usually a negative variable, with  
170 bigger CIN (in absolute value) indicating greater inhibition. On the other hand, CAPE  
171 describes the positive buoyancy of an air particle from the LFC to the equilibrium level  
172 (neutral buoyancy), and can be written as:

$$173 \quad CAPE = - \int_{P_{LFC}}^{P_{EL}} R_d (T_{vp} - T_{ve}) dlnp \quad , \quad (3)$$

174 where  $P_{EL}$  is the pressure at the equilibrium level. Both CIN and CAPE describe the  
175 stability of the atmosphere, and usually convection easily occurs when CAPE is high and  
176 CIN is low (in absolute value; e.g., Colby, 1984; Riemann-Campe et al., 2009; Myoung  
177 and Nielsen-Gammon, 2010a). Note the two variables can sometimes vary in opposite  
178 directions. Indeed, when CAPE is high, strong inhibition may still prohibit the occurrence  
179 of deep convection.

180 In addition, daily and monthly means of horizontal wind speed at 900 hPa,  
181 temperature at 700 hPa ( $T_{700}$ ), 10 m wind speed, dew point temperature ( $T_{dp}$ ), and 2 m air  
182 temperature ( $T_{2m}$ ), total cloud cover, total and convective precipitation are used.

183 Another reanalysis used in this work is the ERA-Interim (Dee et al., 2011) from  
184 the European Centre for Medium-Range Weather Forecasts (ECMWF). ERA-Interim is a  
185 global reanalysis with a horizontal resolution of T255 (about  $0.7^{\circ}$  or 80 km) and 37  
186 vertical levels, available from 1979 to present. It complements the regional reanalysis by  
187 providing a larger domain to analyze circulation variations and also a few surface  
188 variables that are not available in the NARR. 6-hourly analysis and 3-hourly forecast  
189 variables such as surface turbulence stress, vertical and horizontal winds, air temperature,  
190 and specific humidity from 1000 to 200 hPa, 850 hPa winds and geopotential height are  
191 used to calculate daily means of these variables.

192

### 193 **2.5 Multiple-linear regression**

194 To understand the connection between the potentially controlling factors and the  
195 variation of fine dust concentration, multiple-linear regressions are applied by regressing  
196 the observed gridded fine dust concentration onto 3, 4, or 5 standardized controlling  
197 factors, a method similar to the one used by Pu and Ginoux (2017). Here all data are  
198 interpolated to a  $1^{\circ}$  by  $1^{\circ}$  grid for the regression analysis. The fine dust concentration is  
199 then reconstructed by using the regression coefficients and observed variations of the  
200 controlling factors (such as precipitation, surface wind, and bareness). We focus our  
201 analysis on two statistical properties: correlations of regional averaged time series and  
202 pattern correlations for the trends. These two properties are calculated for both observed  
203 and regression model estimated (i.e., reconstructed) fine dust concentrations.

204

### 205 **3. Results**

206 **3.1 Trends of surface fine dust concentration during 1990-2015 and local controlling  
207 factors**

208 Figure 1 shows the trend of fine dust concentration from gridded data (shading)  
209 and also those from stations with at least 23 years of consecutive records (colored circles)  
210 from 1990 to 2015. Significant positive trends are found over the southwestern U.S. in  
211 spring (MAM), over the central to southern Great Plains in summer (JJA), and the  
212 northern Great Plains in fall (SON). Dust concentration also increases over southwestern  
213 Arizona (up to  $0.06 \mu\text{g m}^{-3} \text{ yr}^{-1}$ ), by about 2.5% of its climatological value (Fig. S2 in the  
214 Supplement) per year, in all seasons. A similar increasing trend of fine dust in southern  
215 Arizona in spring from 1988 to 2009 is also noticed by Sorooshian et al. (2011). A  
216 decreasing trend is found over the northeastern U.S. in all seasons as well. The pattern is  
217 somewhat similar to the trend identified by Hand et al. (2017; their Fig. 9) for 2000-2014,  
218 who also found increasing trends of fine dust in the Southwest in spring and the central  
219 Great Plains in summer.

220 As suggested by previous studies, the trend of fine dust may be biased due to  
221 suspicious trends in some chemical species (Al, Si, and Ti) used to construct fine dust in  
222 association with changes of analytical methods (e.g., Hyslop et al., 2015; Hand et al.,  
223 2016; Hand et al., 2017). Fe has been suggested as a good proxy of fine dust since it's  
224 more stable and is a key component of dust (Hand et al. 2016; 2017). We examined the  
225 trend of fine Fe (Fig. S3 in the Supplement), and found the pattern is very similar to the  
226 trend of fine dust. In fact, we found the correlations between seasonal mean fine dust and  
227 Fe (both gridded data and long-term stations) are around 0.90 (significant at the 99%  
228 confidence level) in most part of the U.S. during 1990-2015 (Fig. S4 in the Supplement).

229 This suggests the trends revealed directly from fine dust record are comparably reliable  
230 as those calculated from Fe. So we use fine dust concentration for this analysis.

231 What are the dominant factors influencing the variations of fine dust  
232 concentration? Hand et al. (2016) found that the PDO played an important role in the  
233 variability of fine dust concentration over the Southwest in March by creating a windier,  
234 drier, and less vegetated environment. We would like to extend their analysis to other  
235 seasons and regions. In addition, we focus on identifying key controlling factors at the  
236 local level because remote forcings such as the PDO influence dust variations through  
237 their tele-connection with local controlling factors. Pu and Ginoux (2017) found that  
238 local precipitation, surface bareness, and surface wind speed could explain 49% to 88%  
239 of the variances of dust event frequency (derived from DOD) over the western U.S. and  
240 the Great Plains in different seasons from 2003 to 2015. We first examine to what extent  
241 these factors can explain the variance of near surface fine dust concentration. Similar to  
242 Pu and Ginoux (2017), we do not separate the contribution from local emissions or  
243 remote transportation to the fine dust concentration, although contributions from Asian  
244 dust in spring over the western U.S. (Fischer et al., 2009; Creamean et al., 2014; Yu et al.,  
245 2012) and from North African dust in summer over the southeastern U.S. (Perry et al.,  
246 1997; Prospero, 1999b) have been observed.

247 Figure 2a-d shows the dominant controlling factor among the three (precipitation,  
248 surface wind, and bareness) for fine dust concentration variations at each grid point.  
249 Precipitation plays an important role in most parts of the southern U.S. in winter. In  
250 spring, surface wind starts to dominate the variations of fine dust along the Gulf coast and  
251 eastern Great Plains, consistent with the intensification of the Great Plains low-level jet

252 (e.g., Helfand and Schubert, 1995; Weaver and Nigam, 2008; Pu and Dickinson, 2014; Pu  
253 et al., 2016) in April and May, while bareness is important over the western Great Plains  
254 and the Midwest. During summer, the influence of surface wind speed gets stronger,  
255 especially over western Arizona and the lower Mississippi basin, whereas bareness and  
256 precipitation are also important in many parts of the Great Plains and western U.S.  
257 Precipitation becomes the dominant factor over most parts of the U.S. again in fall, with  
258 surface winds playing a weak role over the southeast and northeast coasts.

259 The regression coefficients obtained here share some similarity with those shown  
260 by Pu and Ginoux, (2017; their Fig 4) using DOD, e.g., the importance of surface  
261 bareness in the Great Plains in spring and summer. However, there are also quite large  
262 differences, likely due to different periods of regression and the fact that the DOD and  
263 surface fine dust concentration are not always linearly related to each other (Fig. S5 in the  
264 Supplement). For instance, over the Great Plains and the southwestern U.S., seasonal  
265 mean fine dust is linearly related to the DOD in spring but not so in summer. As  
266 mentioned earlier, fine dust covers a small fraction of the total mass distribution of dust  
267 particles, thus the connections between fine dust concentration and the controlling factors  
268 could be different from those with the DOD. For example, the scavenging effect of  
269 precipitation is more efficient on small particles (e.g., Zender et al., 2003) and as a result  
270 precipitation generally plays an overall more important role on fine dust variations than  
271 on the DOD, especially in winter, spring, and fall.

272 The correlations between reconstructed fine dust concentration in the  
273 southwestern U.S. (using regression coefficients and observed variations of precipitation,  
274 surface wind, and bareness) and that from the IMPROVE range from 0.69 in fall to 0.82

275 in winter, indicating that the above three factors explain about 48% to 67% variances of  
276 fine dust in the Southwest from 1990 to 2015. Over the Great Plains, correlations  
277 between the reconstructed and observed fine dust concentration ranges from 0.57 in  
278 summer to 0.69 in winter, explaining 32% to 48% variances statistically, lower than over  
279 the Southwest.

280 The pattern correlations between the observed trend and the trend from  
281 reconstructed fine dust are all above 0.80 in the Southwest except in the summer, whereas  
282 in the Great Plains region, the pattern correlations are much lower, from 0.06 in fall to  
283 0.48 in winter. In fact, the reconstructed trend missed the observed positive trend of fine  
284 dust over the central Great Plains in summer (not shown). This is consistent with the low  
285 confidence level of the regression coefficients over the central Great Plains in summer  
286 (Fig. 2c) and indicates that the above three factors are not sufficient to well explain the  
287 variations of fine dust in the central Great Plains.

288 The development of dust storms has long been related to convection and  
289 atmospheric stability (e.g., Marsham et al., 2008; Cuesta et al., 2009). Here we examine  
290 whether the variances of fine dust concentration and trend can be better represented by  
291 adding CIN (i.e., four-factor) and both CIN and CAPE (i.e., five-factor) in addition to the  
292 three factors (i.e., three-factor) discussed above.

293 Figure 2e shows correlations (blue bars) between the observed and the  
294 reconstructed regional mean fine dust concentration from three-, four-, and five-factor  
295 regressions, and corresponding pattern correlations (pink dots) between trends from the  
296 observed and reconstructed fine dust for the Great Plains and the southwestern U.S. In  
297 both regions, correlations of interannual variation between the reconstructed and

298 observed fine dust are slightly improved from three-factor regression to five-factor  
299 regression. Pattern correlations are largely improved over the Great Plains when  
300 including CIN and CAPE, especially in spring (from 0.30 to 0.89) and summer (from  
301 0.34 to 0.93), although slightly decreased in winter, whereas the improvement of pattern  
302 correlations in the Southwest is much weaker.

303 The collinearity among the factors used in the multiple linear regression can be  
304 examined by the variance inflation factor (VIF; O'Brien, 2007; Abudu et al., 2011), and  
305 usually values between 5 and 10 are considered high collinearity and the results of  
306 regression are less reliable. Increasing the number of predictors in multiple linear  
307 regression generally increase VIFs. The VIFs for three-factor regression are around 1 and  
308 2 in most areas, with a few spots around 3 (not shown), while the VIFs for five-factor  
309 regression are slightly higher, especially for CIN and CAPE over the Southwest (Figs. S6  
310 and 7 in the Supplement). The increase of VIF and relatively weak improvement in the  
311 correlations in the Southwest when adding the convective factors suggest that three  
312 factors (precipitation, surface wind and bareness) are sufficient to capture the variations  
313 and trend of fine dust in the region. Over the Great Plains, adding CIN and CAPE can  
314 better explain the variations.

315 We now examine key factors driving the observed positive trends of fine dust  
316 concentration in spring and summer, the dustiest seasons (Fig. S2 in the Supplement),  
317 based on the above analysis. Figure 3a show the trend of observed and reconstructed fine  
318 dust concentrations in spring along with three components contributed to the  
319 reconstructed trend (i.e., from precipitation, bareness, and surface wind). The  
320 reconstructed trend (Reg (all)) largely captures the positive trend in the Southwest shown

321 in the observation (Obs). Among the three factors, precipitation plays the most important  
322 role in contributing to the positive trend over the Southwest, consistent with its dominant  
323 role in explaining observed interannual variability (Fig. 2b). The increase of fine dust is  
324 mainly associated with a decreasing trend of precipitation in the Southwest (Fig. 3b).  
325 Such a drying trend has been related to an increase of anticyclonic conditions in the  
326 North East Pacific (Prein et al., 2016) and an intensification of Pacific trades during  
327 2002-2012 (Delworth et al., 2015).

328 The reconstructed summer trend using coefficients from five-factor regression is  
329 very similar to the observation, with a pattern correlation of 0.95 in the domain (Fig. 4a).  
330 The positive trend over the central Great Plains is largely contributed by CIN, with a  
331 positive center at northern Texas, western Kansas, and Oklahoma. Parts of the positive  
332 trend over Oklahoma and western Kansas are contributed by CAPE. In fact, both CIN  
333 and CAPE have significant negative trends over the central Great Plains, although the  
334 trend of CAPE is slightly weaker than that of CIN (Fig. 4b). A decrease of CIN (i.e., an  
335 increase in its absolute value) denotes an increasing inhibition of convection, while a  
336 weakening of CAPE denotes a **decreasing instability** associated with moist convection.  
337 Note that CIN is also significantly negatively correlated with fine dust concentration on  
338 interannual time scale ( $r = -0.39$ ,  $p = 0.05$ ). This again indicates that CIN plays a more  
339 important role than CAPE in the recent positive trend of fine dust.

340 Both the trends of the CIN and CAPE denote an **increasing** of atmospheric  
341 stability. Changes of CIN and CAPE have been related to boundary layer or near-surface  
342 temperature and moisture (e.g., Ye et al., 1998; Gettelman et al., 2002; Alappattu and  
343 Kunhikrishnan, 2009). Myoung and Nielsen-Gammon (2010b) found that the variations

344 of CIN over Texas in the warm season can be well represented by the differences of  
345 temperature at 700 hPa ( $T_{700}$ ) and surface dew point temperature ( $T_{dp}$ ), i.e.,  $T_{700}-T_{dp}$ .  
346 While  $T_{700}$  is a good proxy for temperature at the free-troposphere below the LFC,  $T_{dp}$   
347 denotes the dryness at the surface. Thus,  $T_{700}-T_{dp}$  represents a joint effect of surface  
348 drying and warming at 700 hPa, a generally stable atmosphere. Here we find both CIN  
349 and CAPE have significant negative correlations with  $T_{700}-T_{dp}$  over the central Great  
350 Plains (Fig. 4c). A significant positive trend of  $T_{700}-T_{dp}$  is also found, supporting the  
351 assumption that the atmospheric stability is enhanced during the period. Such a changes  
352 of stability is largely due to the increase of  $T_{700}$ , although surface drying also contributes.

353 CIN is also found to be significantly correlated with rain days (daily precipitation  
354  $\geq 1 \text{ mm day}^{-1}$ ) in summer in Texas (Myoung and Nielsen-Gammon, 2010b). Here a  
355 similar positive correlation between CIN and rain days in the central Great Plains in also  
356 found from 1990 to 2015 ( $r=0.79$ ,  $p<0.001$ ), suggesting that CIN could influence fine  
357 dust concentration via its connection with rain days. A stable atmosphere prevents deep  
358 moist convection, which reduces the chance of scavenging by precipitation, and also  
359 likely prevents dilution of fine dust concentration in the boundary layer with the clean air  
360 above through convective mixing. The connection underlying CIN and fine dust  
361 concentration is further discussed in section 3.3 using daily data.

362

363 **3.2 The connection between the Great Plains low-level jet and summertime fine dust**  
364 **variations in the central Great Plains (CGP)**

365 An important feature related to the moisture and heat transport and precipitation  
366 in the Great Plains from late spring to summer is the Great Plains low-level jet (LLJ),

367 which develops in April and reaches its maximum wind speed in June and July at around  
368 900 hPa (e.g., Weaver and Nigam, 2008; Pu et al., 2016). The southerly jet covers most of  
369 the southern to central Great Plains, and turns into a westerly around 40° N passing  
370 through the Midwest. How this jet may influence the dust concentration in the CPG in  
371 summer is examined here.

372 Figure 5a shows the time series of the jet index in summer following the  
373 definition of Weaver and Nigam (2008) by averaging 900 hPa meridional wind speed at  
374 the jet core (25°-35°N, 97°-102°W) from 1990 to 2015. The jet index is significantly  
375 positively correlated with fine dust concentration in the CGP ( $r= 0.56$ ,  $p<0.01$ ) and also  
376 has a significant positive trend in summer, suggesting that the jet also contributes to the  
377 increasing of fine dust in the CGP. Such a positive connection between the jet and fine  
378 dust concentration can be explained by jet's negative correlation with CIN and positive  
379 correlation with the near surface wind speed in the CGP (Figs. 5b). An intensified jet  
380 increases the near surface wind speed and meanwhile increases the stability of  
381 atmosphere over the CGP by advecting moisture away to the Midwest and increasing  
382 local temperature via northward warm temperature advection (e.g., Walters and Winkler,  
383 2001; Song et al., 2005; Zhu and Liang, 2013).

384 Because most of the IMPROVE sites (4 out of 6) in the central Great Plains only  
385 have records since 2002, correlations between the jet index and fine dust concentration,  
386 CIN, and surface wind for 2002-2015 are also calculated (Fig. 5c). The patterns are  
387 similar to those during 1990-2015.

388 Dust from Africa can be transported to the southeastern U.S. and even Texas in  
389 summer (e.g., Perry et al., 1997; Prospero, 1999a, b; 2010; 2014; Bozlaker et al., 2013).

390 Does African dust also contribute to the positive trend of fine dust in the CGP via the jet?  
391 Fully addressing this question will require a dust model that can well reproduce the  
392 emission and transport processes of African dust, which is beyond the scope of this paper.  
393 Here we discuss this question based on observational analysis. The regression and trend  
394 analysis above suggests that local atmospheric stability largely contributes to the positive  
395 trend. Since African dust is transported to the continental U.S. passing through the  
396 Caribbean Sea and the Gulf of Mexico, we assume that the variations of fine dust in  
397 stations nearby would reveal the influence of African dust. Two of such stations, VIIS1  
398 (18.3°N, 64.8°W) in the Virgin Islands National Park and EVER1 (25.4°N, 80.7°W) in  
399 the Everglades National Park, are used. It is found that the records from these stations  
400 have significantly positive correlations with fine dust concentration over the southeastern  
401 U.S. in JJA, but not over the CGP (Fig. S8 in the Supplement). This suggests that the  
402 influence of African dust is largely over the Southeast on seasonal mean, consistent with  
403 the results of Hand et al. (2017), who found the influence of North African dust are  
404 mainly over the Southeast, Appalachia, and Virgin islands regions in summer as indicated  
405 by a shift of elemental composition in IMPROVE sites.

406

### 407 **3.3 Factors contributing to high dust concentration over the CGP in summer**

408 While the negative correlation between fine dust concentration and precipitation  
409 in the Southwest is straightforward, the correlation between fine dust and CIN in the CGP  
410 is less obvious. Here we further examine the connection between fine dust and CIN and  
411 other factors associated with high dust concentration in the area using daily events. As

412 mentioned earlier, since most stations in the CGP have records since 2002, the following  
413 analysis focuses on summer during 2002-2015.

414

415 **3.3.1 Connection between fine dust concentration and CIN**

416 Figures 6a-c show the scatter plot of standardized (means are removed and then  
417 divided by one standard deviation) CIN and friction velocity ( $U^*$ ) anomalies, for all the  
418 days in summer from 2002 to 2015, days when IMPROVE records are available (431  
419 days), and dusty days, defined as days when daily anomaly of IMPROVE observation is  
420 greater than one standard deviation (52 days), respectively.  $U^*$  is defined as the  
421 following,

422 
$$U^* = ([\tau/\rho])^{1/2} = [(\overline{u'w'})^2 + (\overline{v'w'})^2]^{1/4} , \quad (4)$$

423 where  $\tau$  is the Reynolds stress and  $\rho$  is air density, and  $\overline{u'w'}$  and  $\overline{v'w'}$  are vertical flux of  
424 horizontal momentum. We calculated  $U^*$  using the surface turbulence stresses ( $-\rho\overline{u'w'}$ ,  
425  $-\rho\overline{v'w'}$ ) from the ERA-Interim.  $U^*$  has long been related to dust emission (e.g., Gillette  
426 and Passi, 1988; Marticorena and Bergametti, 1995; Zender et al., 2003). As shown in Fig.  
427 6, CIN is significantly negatively related to the friction velocity, which is associated with  
428 turbulent fluctuations in the boundary layer. This indicates a large negative CIN, or great  
429 inhibition for convection, is related to stronger near surface turbulence fluxes and  $U^*$ .  
430 Such a negative connection is robust both in days with fine dust records and in dusty  
431 days. CIN represents the integrated inhibition from the surface to LFC (Eq. 2), then how  
432 does CIN relate to surface turbulence fluxes and  $U^*$ ?

433 In the CGP, CIN is significantly negatively correlated with near surface  
434 temperature,  $T_{2m}$ , i.e., a strong inhibition is associated with higher  $T_{2m}$ , for all days in JJA

435 and for days when fine dust records are available (Table 1). This is consistent with  
436 previous study over Texas (Myoung and Nielsen-Gammon, 2010b). Meanwhile,  $U^*$  is  
437 significantly positively correlated with  $T_{2m}$  (Table 1), indicating that CIN is connected  
438 with  $U^*$  via its connection with near surface temperature. Also, note such a connection  
439 seems not valid during dusty days (correlation between  $T_{2m}$  and  $U^*$  is not significant).  
440 Similarly, we found a close connection among CIN,  $T_{700}$ - $T_{dp}$ , and  $U^*$  (Table 1). This  
441 again, suggests that CIN can influence  $U^*$  via its connection with surface variables such  
442 as temperature and dryness. Variables in Table 1 are all from the ERA-Interim (except  
443 CIN) to be consistent with  $U^*$ , results are similar if using NARR variables.

444 One hypothesis for the connection between CIN and  $U^*$  for dusty days is shown in  
445 Table 2. A significant positive correlation between CIN and vertical wind at 850 hPa  
446 ( $w_{850}$ ) is found, indicating that when the inhibition is strong, it favors subsidence. This is  
447 consistent with the finding by Riemann-Campe et al. (2009) who found in climatology  
448 high CIN value is located over subtropical regions with strong subsidence. The  
449 subsidence may transports momentum downward and promotes  $U^*$ . This is consistent  
450 with the negative correlation between  $U^*$  and  $w_{850}$  (Table 2). However, we also notice  
451 that the above connections in dusty days are not valid in the NARR, suggesting further  
452 investigation on this mechanism is needed.

453 Despite the connection between CIN and surface variables, the possible  
454 mechanism that strong inhibition prevents dilution is also examined. We found four  
455 examples in CALIOP snapshots over the CGP when the daily anomaly of near surface  
456 fine dust concentration from the IMPROVE network is greater than one standard  
457 deviation. Figure 7 shows nighttime 532 nm total attenuated backscatter (shading) on

458 August 10<sup>th</sup>, 2007 (top) and on June 21<sup>st</sup>, 2013 (bottom). Black contours show area with  
459 depolarization ratio  $\geq 0.2$ , denoting dust aerosols. In both cases, the inhibition is quite  
460 strong, with CIN anomaly greater than one standard deviation. The difference between  
461 the two cases is that on June 21<sup>st</sup>, 2013, CAPE is higher, which leads to some convection  
462 as denoted by the clouds above. However, in both cases, with strong inhibition, dust  
463 particles are largely located in a layer between the surface and 2 km. Figure 8 shows a  
464 different situation when CIN has positive anomaly (i.e., weak inhibition). In these cases,  
465 dust particle extends up to 4 km, and surface fine dust concentrations in the CGP (with  
466 anomalies of 2.3 and 2.1  $\mu\text{g m}^{-3}$ ) are also lower than those in Fig. 7 (with anomalies of  
467 4.0 and 7.1  $\mu\text{g m}^{-3}$ ). Nonetheless, more cases are needed to further verify this mechanism.

468

### 469 **3.3.2 Large-scale circulation pattern in dusty days**

470 Figure 9 shows the daily composites of related metrological variables in dusty  
471 days, i.e., when daily anomaly of CGP fine dust concentration is greater than one  
472 standard deviation. Anomalous high fine dust concentration is associated with a reduced  
473 CIN (Fig. 9b) in the CGP, but not so much with CAPE (Fig. 9c). CAPE is anomalously  
474 enhanced over the northern Plains and the Midwest. Both the LLJ, near surface wind, and  
475 friction velocity are enhanced (Figs. 9d-f). Precipitation (mostly convective precipitation)  
476 in the CGP also decreases with reduced cloud cover, but increases in the north (Figs. 9g-  
477 i), consistent with enhanced CAPE there. These features are quite consistent with our  
478 analysis above on the favorable condition of enhanced fine dust in the CGP.

479 Figure 10 shows the composites of vertical velocity (shading), vertical and  
480 meridional wind vectors, specific humidity (purple contours), and potential temperature

481 (grey contours) zonally averaged over the central Great Plains ( $95^{\circ}$  - $102^{\circ}$  W), along with  
482 fine dust concentration (orange line). Anomalous dry subsidence is centered at  $30^{\circ}$ - $36^{\circ}$ N,  
483 with anomalous southerly winds at low-level associated with an intensified jet, while a  
484 rising motion of moist air is located around  $38$ - $42^{\circ}$ N with a maximum at 700-400 hPa.  
485 The dipole pattern of anomalous vertical velocity is consistent with the precipitation  
486 anomaly in the area (Figs. 9g-h). The anomalous potential temperature contour is quite  
487 uniform near the surface at  $30^{\circ}$ - $36^{\circ}$ N with an inversion around 700 hPa, indicating a  
488 well-mixed boundary layer in the region with increased fine dust.

489 What causes the changes of atmospheric stability, precipitation, and winds?  
490 Figure 11 shows the composites of  $T_{2m}$  and geopotential height and winds at 850 hPa  
491 during dusty days. Following Li et al. (2012a), 1560 gpm contour is used here to denote  
492 the western edge of the North Atlantic subtropical high in the 2002-2015 climatology  
493 (blue) and in dusty days (red). A westward extension of the subtropical high during dust  
494 days is quite evident, with enhanced geopotential height over the southeastern U.S. and  
495 the Gulf of Mexico (Fig. 11b). Such a westward extension of the subtropical high  
496 intensifies the LLJ by increasing the zonal pressure gradient, and also contributes to the  
497 anomalous precipitation and vertical velocity patterns, as similar patterns are found in  
498 previous studies associated with a westward extension of the subtropical high (e.g., Li et  
499 al., 2012a; their Figs. 3a and 4a). The formation of the North Atlantic subtropical high  
500 has been related to the land-sea heating contrast (Wu and Liu, 2003; Liu et al.,  
501 2004; Miyasaka and Nakamura, 2005; Li et al., 2012a; Li et al., 2012b). One possible  
502 reason of the westward extension of the subtropical high is the anomalous surface

503 warming over large part of the central and eastern U.S. (Fig. 11a) in dusty days that  
504 enhances the land-sea temperature gradient.

505

506 **4. Conclusions**

507 Fine dust is an important component in the total PM 2.5 mass in the western to  
508 central U.S. in spring and summer (Hand et al. 2017). Previous studies found positive  
509 trends of fine dust concentration in the southwestern U.S. in spring and the central U.S. in  
510 summer in the past 20 years (Hand et al., 2016;2017;Zhang et al., 2017), but the  
511 underlying causes are not clear, especially for the positive trend over the central U.S.  
512 This study examined local controlling factors associated with variations of fine dust  
513 concentration from Interagency Monitoring of Protected Visual Environments  
514 (IMPROVE) stations for 1990-2015 in each season. While precipitation, surface  
515 bareness, and wind speed largely control the variation of fine dust concentration in the  
516 southwestern U.S., including two convective parameters, convective inhibition (CIN) and  
517 convective available potential energy (CAPE) better explains the variations over the  
518 Great Plains from spring to fall. In particular, we found that the increasing trend of fine  
519 dust concentration over the Southwest in spring is associated with a significantly  
520 decreasing trend of precipitation, while the positive trend of fine dust over the central  
521 Great Plains (CGP) is largely due to enhanced atmospheric stability revealed by an  
522 enhancing of CIN (greater inhibition) and a decreasing of CAPE. Such a stability change  
523 is associated with surface drying and warming in the lower troposphere around 700 hPa,  
524 i.e., a positive trend of  $T_{700} - T_{dp}$ . A stable atmosphere prevents moist convection that can  
525 remove fine dust by in-cloud or precipitation scavenging and also likely prevent the

526 dilution of fine dust concentration by prohibiting convective mixing between the dusty  
527 boundary layer air and the clean air above.

528 The variations of the fine dust concentration in the CGP are also significantly  
529 correlated to the Great Plains low-level jet, with a stronger jet corresponding to higher  
530 fine dust concentration. Such a connection is largely due to jet's positive correlation with  
531 surface wind speed and negative correlation with CIN.

532 The influence of CIN on dust emission is examined using daily data in summer. It  
533 is found that CIN is significantly negatively related to surface friction velocity ( $U^*$ ), i.e.,  
534 with greater inhibition in association with stronger  $U^*$ . Such a connection is largely due  
535 to CIN's connection with surface variables such as 2m temperature and dew point  
536 temperature. During dusty days, another possible connection is that the anomalous  
537 subsidence associated with strong inhibition may transport momentum downward and  
538 increase surface  $U^*$ .

539 Dusty days in the CGP in summer are associated with a westward extension of the  
540 North Atlantic subtropical high that intensifies the Great Plains low-level jet and surface  
541 wind speed, increases atmospheric stability, and also creates anomalous subsidence over  
542 the southern to central Great Plains and the Southeast and rising motion over the  
543 Midwest, and correspondingly a south-north dipole pattern of precipitation anomaly. The  
544 westward extension of the subtropical high is likely associated with the anomalous  
545 surface warming over the central to eastern U.S.

546 Our findings have important implications for future projections of fine dust  
547 variation in the U.S. Climate models have projected drying trends over the southwestern  
548 and the central U.S. (e.g., Seager et al., 2007; Cook et al., 2015) as well as an

549 intensification of the North Atlantic subtropical high (Li et al., 2012b) in the late 21<sup>st</sup>  
550 century, all favorable to an increase of fine dust in the Southwest and central Great  
551 Plains. Whether current increasing trends of fine dust will persist into the future requires  
552 further investigations that include factors not discussed here such as changes of  
553 anthropogenic land use, local synoptic-scale systems (e.g., cyclones and fronts), and  
554 remote forcings.

555

556

557

558

559

560

561

562

563

564

565

566

567

568

569

570

571

572 *Acknowledgements.*

573 IMPROVE is a collaborative association of state, tribal, and federal agencies, and  
574 international partners. US Environmental Protection Agency is the primary funding  
575 source, with contracting and research support from the National Park Service. The Air  
576 Quality Group at the University of California, Davis is the central analytical laboratory,  
577 with ion analysis provided by Research Triangle Institute, and carbon analysis provided  
578 by Desert Research Institute. IMPROVE fine dust data is downloaded from  
579 <http://views.cira.colostate.edu/fed/DataWizard/>. AVHRR leaf area index data are  
580 available at: <ftp://eclipse.ncdc.noaa.gov/pub/cdr/lai-fapar/files/>. PRECL Precipitation  
581 data are provided by the NOAA/OAR/ESRL PSD, Boulder, Colorado, USA, from their  
582 web site at <http://www.esrl.noaa.gov/psd/>. The CALIPSO products are downloaded from  
583 [https://www-calipso.larc.nasa.gov/tools/data\\_avail/dpo\\_read.php?y=2007&m=08&d=10](https://www-calipso.larc.nasa.gov/tools/data_avail/dpo_read.php?y=2007&m=08&d=10).  
584 The NCEP/NCAR reanalysis product is obtained from  
585 <http://www.esrl.noaa.gov/psd/data/gridded/data.ncep.reanalysis.html> and the ERA-  
586 Interim is downloaded from <http://www.ecmwf.int/en/research/climate-reanalysis/era->  
587 interim. The NARR reanalysis is downloaded from  
588 <https://www.esrl.noaa.gov/psd/data/gridded/data.narr.html>. This research is supported by  
589 NOAA and Princeton University's Cooperative Institute for Climate Science and NASA  
590 under grant NNH14ZDA001N-ACMAP. The authors thank Drs. Stuart Evans and Jordan  
591 Schnell for their helpful comments on the early version of this paper.  
592  
593  
594

## References

596 Abudu, S., Cui, C. L., King, J. P., Moreno, J., and Bawazir, A. S.: Modeling of daily pan  
597 evaporation using partial least squares regression, *Sci China Technol Sc*, 54, 163-  
598 174, 10.1007/s11431-010-4205-z, 2011.

599 Alappattu, D. P., and Kunhikrishnan, P. K.: Premonsoon estimates of convective  
600 available potential energy over the oceanic region surrounding the Indian  
601 subcontinent, *J Geophys Res-Atmos*, 114, 10.1029/2008jd011521, 2009.

602 Bozlaker, A., Prospero, J. M., Fraser, M. P., and Chellam, S.: Quantifying the  
603 Contribution of Long-Range Saharan Dust Transport on Particulate Matter  
604 Concentrations in Houston, Texas, Using Detailed Elemental Analysis, *Environ  
605 Sci Technol*, 47, 10179-10187, 10.1021/es4015663, 2013.

606 Chen, M. Y., Xie, P. P., Janowiak, J. E., and Arkin, P. A.: Global land precipitation: A  
607 50-yr monthly analysis based on gauge observations, *J Hydrometeorol*, 3, 249-  
608 266, Doi 10.1175/1525-7541(2002)003<0249:Glpaym>2.0.Co;2, 2002.

609 Claverie, M., Vermote, E., and NOAA-CDR-Program: NOAA Climate Data Record  
610 (CDR) of Leaf Area Index (LAI) and Fraction of Absorbed Photosynthetically  
611 Active Radiation (FAPAR), Version 4, NOAA National Climatic Data Center,  
612 10.7289/V5M043BX, 2014.

613 Claverie, M., Matthews, J. L., Vermote, E. F., and Justice, C. O.: A 30+ Year AVHRR  
614 LAI and FAPAR Climate Data Record: Algorithm Description and Validation,  
615 *Remote Sens-Basel*, 8, 10.3390/rs8030263, 2016.

616 Colby, F. P.: Convective Inhibition as a Predictor of Convection during Ave-Sesame-II,  
617 *Mon Weather Rev*, 112, 2239-2252, Doi 10.1175/1520-  
618 0493(1984)112<2239:Ciaapo>2.0.Co;2, 1984.

619 Cook, B. I., Ault, T. R., and Smerdon, J. E.: Unprecedented 21st century drought risk in  
620 the American Southwest and Central Plains, *Science Advances*, 1, 1-7,  
621 10.1126/sciadv.1400082 2015.

622 Creamean, J. M., Spackman, J. R., Davis, S. M., and White, A. B.: Climatology of long-  
623 range transported Asian dust along the West Coast of the United States, *J  
624 Geophys Res-Atmos*, 119, 12171-12185, 10.1002/2014jd021694, 2014.

625 Crooks, J. L., Cascio, W. E., Percy, M. S., Reyes, J., Neas, L. M., and Hilborn, E. D.: The  
626 Association between Dust Storms and Daily Non-Accidental Mortality in the  
627 United States, 1993-2005, *Environ Health Persp*, 124, 1735-1743,  
628 10.1289/Ehp216, 2016.

629 Cuesta, J., Marsham, J. H., Parker, D. J., and Flamant, C.: Dynamical mechanisms  
630 controlling the vertical redistribution of dust and the thermodynamic structure of  
631 the West Saharan atmospheric boundary layer during summer, *Atmos Sci Lett*,  
632 10, 34-42, 10.1002/asl.207, 2009.

633 Dee, D. P., Uppala, S. M., Simmons, A. J., Berrisford, P., Poli, P., Kobayashi, S., Andrae,  
634 U., Balmaseda, M. A., Balsamo, G., Bauer, P., Bechtold, P., Beljaars, A. C. M.,  
635 van de Berg, L., Bidlot, J., Bormann, N., Delsol, C., Dragani, R., Fuentes, M.,  
636 Geer, A. J., Haimberger, L., Healy, S. B., Hersbach, H., Holm, E. V., Isaksen, L.,  
637 Kallberg, P., Kohler, M., Matricardi, M., McNally, A. P., Monge-Sanz, B. M.,  
638 Morcrette, J. J., Park, B. K., Peubey, C., de Rosnay, P., Tavolato, C., Thepaut, J.  
639 N., and Vitart, F.: The ERA-Interim reanalysis: configuration and performance of  
640 the data assimilation system, *Q J Roy Meteor Soc*, 137, 553-597, 10.1002/qj.828,  
641 2011.

642 Delworth, T. L., Zeng, F. R., Rosati, A., Vecchi, G. A., and Wittenberg, A. T.: A Link  
643 between the Hiatus in Global Warming and North American Drought, *J Climate*,  
644 28, 3834-3845, 10.1175/Jcli-D-14-00616.1, 2015.

645 Duce, R. A.: Sources, distributions, and fluxes of mineral aerosols and their relationship  
646 to climate, in: *Dalhem Workshop on Aerosol Forcing of Climate*, edited by:  
647 Charlson, R. J., and Heintzenberg, J., John Wiley, New York, 43-72, 1995.

648 Fischer, E. V., Hsu, N. C., Jaffe, D. A., Jeong, M. J., and Gong, S. L.: A decade of dust:  
649 Asian dust and springtime aerosol load in the US Pacific Northwest, *Geophys Res  
650 Lett*, 36, 10.1029/2008gl036467, 2009.

651 Gettelman, A., Seidel, D. J., Wheeler, M. C., and Ross, R. J.: Multidecadal trends in  
652 tropical convective available potential energy, *J Geophys Res-Atmos*, 107,  
653 10.1029/2001jd001082, 2002.

654 Gillette, D. A., and Passi, R.: Modeling Dust Emission Caused by Wind Erosion, *J  
655 Geophys Res-Atmos*, 93, 14233-14242, DOI 10.1029/JD093iD11p14233, 1988.

656 Ginoux, P., Prospero, J. M., Gill, T. E., Hsu, N. C., and Zhao, M.: Global-Scale  
657 Attribution of Anthropogenic and Natural Dust Sources and Their Emission Rates  
658 Based on Modis Deep Blue Aerosol Products, *Rev Geophys*, 50,  
659 10.1029/2012rg000388, 2012.

660 Hand, J. L., Copeland, S. A., Day, D. E., Dillner, A. M., Indresand, H., Malm, W. C.,  
661 McDade, C. E., Moore, C. T., Pitchford, M. L., Schichtel, B. A., and Watson, J.  
662 G.: IMPROVE (Interagency Monitoring of Protected Visual Environments):  
663 Spatial and seasonal patterns and temporal variability of haze and its constituents  
664 in the United States, 2011.

665 Hand, J. L., Schichtel, B. A., Pitchford, M., Malm, W. C., and Frank, N. H.: Seasonal  
666 composition of remote and urban fine particulate matter in the United States, *J*  
667 *Geophys Res-Atmos*, 117, 10.1029/2011jd017122, 2012.

668 Hand, J. L., White, W. H., Gebhart, K. A., Hyslop, N. P., Gill, T. E., and Schichtel, B. A.:  
669 Earlier onset of the spring fine dust season in the southwestern United States,  
670 *Geophys Res Lett*, 43, 4001-4009, 10.1002/2016gl068519, 2016.

671 Hand, J. L., Gill, T. E., and Schichtel, B. A.: Spatial and seasonal variability in fine  
672 mineral dust and coarse aerosol mass at remote sites across the United States, *J*  
673 *Geophys Res-Atmos*, 122, 3080-3097, 10.1002/2016jd026290, 2017.

674 Helfand, H. M., and Schubert, S. D.: Climatology of the Simulated Great-Plains Low-  
675 Level Jet and Its Contribution to the Continental Moisture Budget of the United-  
676 States, *J Climate*, 8, 784-806, Doi 10.1175/1520-  
677 0442(1995)008<0784:Cotsgp>2.0.Co;2, 1995.

678 Hyslop, N. P., Trzepla, K., and White, W. H.: Assessing the Suitability of Historical  
679 PM2.5 Element Measurements for Trend Analysis, *Environ Sci Technol*, 49,  
680 9247-9255, 10.1021/acs.est.5b01572, 2015.

681 Kok, J. F.: A scaling theory for the size distribution of emitted dust aerosols suggests  
682 climate models underestimate the size of the global dust cycle, *P Natl Acad Sci*  
683 USA, 108, 1016-1021, 10.1073/pnas.1014798108, 2011.

684 Li, F. Y., Ginoux, P., and Ramaswamy, V.: Transport of Patagonian dust to Antarctica, *J*  
685 *Geophys Res-Atmos*, 115, 10.1029/2009jd012356, 2010.

686 Li, L. F., Li, W. H., and Kushnir, Y.: Variation of the North Atlantic subtropical high  
687 western ridge and its implication to Southeastern US summer precipitation, *Clim  
688 Dynam*, 39, 1401-1412, 10.1007/s00382-011-1214-y, 2012a.

689 Li, W. H., Li, L. F., Ting, M. F., and Liu, Y. M.: Intensification of Northern Hemisphere  
690 subtropical highs in a warming climate, *Nat Geosci*, 5, 830-834,  
691 10.1038/Ngeo1590, 2012b.

692 Liu, Y. M., Wu, G. X., and Ren, R. C.: Relationship between the subtropical anticyclone  
693 and diabatic heating, *J Climate*, 17, 682-698, Doi 10.1175/1520-  
694 0442(2004)017<0682:Rbtsaa>2.0.Co;2, 2004.

695 Malm, W. C., Sisler, J. F., Huffman, D., Eldred, R. A., and Cahill, T. A.: Spatial and  
696 Seasonal Trends in Particle Concentration and Optical Extinction in the United-  
697 States, *J Geophys Res-Atmos*, 99, 1347-1370, Doi 10.1029/93jd02916, 1994.

698 Marsham, J. H., Parker, D. J., Grams, C. M., Taylor, C. M., and Haywood, J. M.: Uplift  
699 of Saharan dust south of the intertropical discontinuity, *J Geophys Res-Atmos*,  
700 113, 10.1029/2008jd009844, 2008.

701 Marticorena, B., and Bergametti, G.: Modeling the Atmospheric Dust Cycle .1. Design of  
702 a Soil-Derived Dust Emission Scheme, *J Geophys Res-Atmos*, 100, 16415-16430,  
703 Doi 10.1029/95jd00690, 1995.

704 Mesinger, F., DiMego, G., Kalnay, E., Mitchell, K., Shafran, P. C., Ebisuzaki, W., Jovic,  
705 D., Woollen, J., Rogers, E., Berbery, E. H., Ek, M. B., Fan, Y., Grumbine, R.,  
706 Higgins, W., Li, H., Lin, Y., Manikin, G., Parrish, D., and Shi, W.: North  
707 American regional reanalysis, *B Am Meteorol Soc*, 87, 343-360, 10.1175/Bams-  
708 87-3-343, 2006.

709 Miyasaka, T., and Nakamura, H.: Structure and formation mechanisms of the northern  
710 hemisphere summertime subtropical highs, *J Climate*, 18, 5046-5065, Doi  
711 10.1175/Jcli3599.1, 2005.

712 Morman, S. A., and Plumlee, G. S.: The role of airborne mineral dusts in human disease,  
713 *Aeolian Res*, 9, 203-212, 10.1016/j.aeolia.2012.12.001, 2013.

714 Myoung, B., and Nielsen-Gammon, J. W.: Sensitivity of Monthly Convective  
715 Precipitation to Environmental Conditions, *J Climate*, 23, 166-188,  
716 10.1175/2009jcli2792.1, 2010a.

717 Myoung, B., and Nielsen-Gammon, J. W.: The Convective Instability Pathway to Warm  
718 Season Drought in Texas. Part I: The Role of Convective Inhibition and Its  
719 Modulation by Soil Moisture, *J Climate*, 23, 4461-4473, 10.1175/2010jcli2946.1,  
720 2010b.

721 O'Brien, R. M.: A caution regarding rules of thumb for variance inflation factors, *Qual  
722 Quant*, 41, 673-690, 10.1007/s11135-006-9018-6, 2007.

723 Perry, K. D., Cahill, T. A., Eldred, R. A., Dutcher, D. D., and Gill, T. E.: Long-range  
724 transport of North African dust to the eastern United States, *J Geophys Res-  
725 Atmos*, 102, 11225-11238, Doi 10.1029/97jd00260, 1997.

726 Prein, A. F., Holland, G. J., Rasmussen, R. M., Clark, M. P., and Tye, M. R.: Running  
727 dry: The US Southwest's drift into a drier climate state, *Geophys Res Lett*, 43,  
728 1272-1279, 10.1002/2015gl066727, 2016.

729 Prospero, J. M.: Long-term measurements of the transport of African mineral dust to the  
730 southeastern United States: Implications for regional air quality, *J Geophys Res-  
731 Atmos*, 104, 15917-15927, Doi 10.1029/1999jd900072, 1999a.

732 Prospero, J. M.: Long-range transport of mineral dust in the global atmosphere: Impact of  
733 African dust on the environment of the southeastern United States, P Natl Acad  
734 Sci USA, 96, 3396-3403, DOI 10.1073/pnas.96.7.3396, 1999b.

735 Prospero, J. M., Landing, W. M., and Schulz, M.: African dust deposition to Florida:  
736 Temporal and spatial variability and comparisons to models, J Geophys Res-  
737 Atmos, 115, 10.1029/2009jd012773, 2010.

738 Prospero, J. M., Collard, F. X., Molinie, J., and Jeannot, A.: Characterizing the annual  
739 cycle of African dust transport to the Caribbean Basin and South America and its  
740 impact on the environment and air quality, Global Biogeochem Cy, 28, 757-773,  
741 10.1002/2013gb004802, 2014.

742 Pu, B., and Dickinson, R. E.: Diurnal Spatial Variability of Great Plains Summer  
743 Precipitation Related to the Dynamics of the Low-Level Jet, J Atmos Sci, 71,  
744 1807-1817, 10.1175/Jas-D-13-0243.1, 2014.

745 Pu, B., Dickinson, R. E., and Fu, R.: Dynamical connection between Great Plains low-  
746 level winds and variability of central Gulf States precipitation, J Geophys Res-  
747 Atmos, 121, 3421-3434, 10.1002/2015jd024045, 2016.

748 Pu, B., and Ginoux, P.: Projection of American dustiness in the late 21st century due to  
749 climate change, Scientific Reports, 7:5553, 1-10, 10.1038/s41598-017-05431-9,  
750 2017.

751 Reid, J. S., Jonsson, H. H., Maring, H. B., Smirnov, A., Savoie, D. L., Cliff, S. S., Reid,  
752 E. A., Livingston, J. M., Meier, M. M., Dubovik, O., and Tsay, S. C.: Comparison  
753 of size and morphological measurements of coarse mode dust particles from  
754 Africa, J Geophys Res-Atmos, 108, 10.1029/2002jd002485, 2003.

755 Riemann-Campe, K., Fraedrich, K., and Lunkeit, F.: Global climatology of Convective  
756 Available Potential Energy (CAPE) and Convective Inhibition (CIN) in ERA-40  
757 reanalysis, *Atmos Res*, 93, 534-545, 10.1016/j.atmosres.2008.09.037, 2009.

758 Ruane, A. C.: NARR's Atmospheric Water Cycle Components. Part I: 20-Year Mean and  
759 Annual Interactions, *J Hydrometeorol*, 11, 1205-1219, 10.1175/2010jhm1193.1,  
760 2010a.

761 Ruane, A. C.: NARR's Atmospheric Water Cycle Components. Part II: Summertime  
762 Mean and Diurnal Interactions, *J Hydrometeorol*, 11, 1220-1233,  
763 10.1175/2010jhm1279.1, 2010b.

764 Ruiz-Barradas, A., and Nigam, S.: Great plains hydroclimate variability: The view from  
765 North American regional reanalysis, *J Climate*, 19, 3004-3010, Doi  
766 10.1175/Jcli3768.1, 2006.

767 Sassen, K.: The Polarization Lidar Technique for Cloud Research - a Review and Current  
768 Assessment, *B Am Meteorol Soc*, 72, 1848-1866, Doi 10.1175/1520-  
769 0477(1991)072<1848:Tpltfc>2.0.Co;2, 1991.

770 Seager, R., Ting, M. F., Held, I., Kushnir, Y., Lu, J., Vecchi, G., Huang, H. P., Harnik,  
771 N., Leetmaa, A., Lau, N. C., Li, C. H., Velez, J., and Naik, N.: Model projections  
772 of an imminent transition to a more arid climate in southwestern North America,  
773 *Science*, 316, 1181-1184, 10.1126/science.1139601, 2007.

774 Song, J., Liao, K., Coulter, R. L., and Lesht, B. M.: Climatology of the low-level jet at  
775 the southern Great Plains atmospheric Boundary Layer Experiments site, *J Appl*  
776 *Meteorol*, 44, 1593-1606, Doi 10.1175/Jam2294.1, 2005.

777 Sorooshian, A., Wonaschutz, A., Jarjour, E. G., Hashimoto, B. I., Schichtel, B. A., and  
778 Betterton, E. A.: An aerosol climatology for a rapidly growing arid region  
779 (southern Arizona): Major aerosol species and remotely sensed aerosol properties,  
780 *J Geophys Res-Atmos*, 116, 10.1029/2011jd016197, 2011.

781 Tong, D. Q., Wang, J. X. L., Gill, T. E., Lei, H., and Wang, B. Y.: Intensified dust storm  
782 activity and Valley fever infection in the southwestern United States, *Geophys*  
783 *Res Lett*, 44, 4304-4312, 10.1002/2017gl073524, 2017.

784 Walters, C. K., and Winkler, J. A.: Airflow configurations of warm season southerly low-  
785 level wind maxima in the Great Plains. Part I: spatial and temporal characteristics  
786 and relationship to convection, *Weather Forecast*, 16, 513-530, Doi  
787 10.1175/1520-0434(2001)016<0513:Acowss>2.0.Co;2, 2001.

788 Weaver, S. J., and Nigam, S.: Variability of the great plains low-level jet: Large-scale  
789 circulation context and hydroclimate impacts, *J Climate*, 21, 1532-1551,  
790 10.1175/2007jcli1586.1, 2008.

791 Winker, D. M., Hunt, W., and Hostetler, C.: Status and performance of the CALIOP  
792 lidar, *Bba Lib*, 5575, 8-15, 10.1117/12.571955, 2004.

793 Winker, D. M., Hunt, W. H., and McGill, M. J.: Initial performance assessment of  
794 CALIOP, *Geophys Res Lett*, 34, 10.1029/2007gl030135, 2007.

795 Wu, G. X., and Liu, Y. M.: Summertime quadruplet heating pattern in the subtropics and  
796 the associated atmospheric circulation, *Geophys Res Lett*, 30,  
797 10.1029/2002gl016209, 2003.

798 Ye, B., Del Genio, A. D., and Lo, K. K. W.: CAPE variations in the current climate and  
799 in a climate change, *J Climate*, 11, 1997-2015, Doi 10.1175/1520-0442-  
800 11.8.1997, 1998.

801 Yu, H. B., Remer, L. A., Chin, M., Bian, H. S., Tan, Q., Yuan, T. L., and Zhang, Y.:  
802 Aerosols from Overseas Rival Domestic Emissions over North America, *Science*,  
803 337, 566-569, 10.1126/science.1217576, 2012.

804 Zender, C. S., Bian, H. S., and Newman, D.: Mineral Dust Entrainment and Deposition  
805 (DEAD) model: Description and 1990s dust climatology, *J Geophys Res-Atmos*,  
806 108, 10.1029/2002jd002775, 2003.

807 Zhang, L., Henze, D. K., Grell, G. A., Torres, O., Jethva, H., and Lamsal, L. N.: What  
808 factors control the trend of increasing AAOD over the United States in the last  
809 decade?, *J. Geophys. Res. Atmos.*, 122, 1797-1810, 10.1002/2016JD025472,  
810 2017.

811 Zhu, J. H., and Liang, X. Z.: Impacts of the Bermuda High on Regional Climate and  
812 Ozone over the United States, *J Climate*, 26, 1018-1032, 10.1175/Jcli-D-12-  
813 00168.1, 2013.

814

815

816

817

818 Table 1 Correlations between friction velocity ( $U^*$ ) and CIN, CIN and 2 meter  
819 temperature ( $T_{2m}$ ),  $T_{2m}$  and  $U^*$ ,  $T_{700}-T_{dp}$  (the differences between air temperature at 700  
820 hPa and 2m dew point temperature) and CIN,  $T_{700}-T_{dp}$  and  $U^*$  for all days in JJA from  
821 2002 to 2015 (1288 days), days when fine dust concentration is available (431 days), and  
822 dusty days (52 days). All values are significant at the 95% confidence level (t-test) except  
823 those listed in italic.

824

825 Table 2 Correlations between  $U^*$  and CIN, CIN and vertical wind speed at 850 hPa  
826 ( $w_{850}$ ),  $w_{850}$  and  $U^*$  during dusty days in JJA from 2002 to 2015. All values are  
827 significant at the 95% confidence level except the value significant at the 90% confidence  
828 level is labeled with a “+” (t-test).

829

830

831

832

833

834

835

836

837

838

839

840

841 Figure 1. Trend (shading) of fine dust concentration ( $\mu\text{g m}^{-3}$ ) from 1990 to 2015 in (a)  
842 DJF, (b) MAM, (c) JJA, and (d) SON from IMPROVE gridded data. Dotted areas are  
843 significant at the 95% confidence level. The colored circles show the trend at IMPROVE  
844 stations with consecutive records for at least 23 years during 1990-2015. Circles with  
845 green outlines denote that the trend is significant at the 90% confidence level. Black  
846 boxes denote the averaging areas of the southwestern U.S. (left) and the Great Plains  
847 (right).

848

849 Figure 2. (a)-(d) Multiple linear regression coefficients calculated by regressing fine dust  
850 concentration from 1990-2015 onto standardized precipitation (purple), bareness  
851 (orange), and surface wind (green). Color denotes the most influential factor at each grid  
852 (i.e., the largest regression coefficient in absolute value among the three), while  
853 saturation of the color shows the magnitude of the coefficient (0 to 0.3). Areas significant  
854 at the 95% confidence levels are dotted. (e) Bar-plot showing the correlations between  
855 observed regional mean fine dust concentration and the reconstructed concentration using  
856 3, 4, and 5 controlling factors (light, median, and deep blue), and pattern correlation  
857 between trends from the observation and from reconstructed fine dust using 3, 4, and 5  
858 factors (light, medium, and deep pink) in the Great Plains (GP) and the southwestern U.S.  
859 (WST, black boxes in Fig. 1). “3-factor” denotes precipitation, bareness, and surface  
860 wind, “4-factor” denotes precipitation, bareness, surface wind, and CIN, “5-factor”  
861 denotes precipitation, bareness, surface wind, CIN, and CAPE.

862

863 Figure 3. (a) Observed (Obs) and reconstructed (Reg) trends of fine dust concentration  
864 ( $\mu\text{g m}^{-3}$ ) using three factors in spring from 1990 to 2015. The contributions from each  
865 factor (precipitation, bareness, and surface wind) to the overall reconstructed trend are  
866 also shown (second row). Dotted areas are significant at the 90% confidence level.  
867 Pattern correlation between reconstructed dust concentration trends and observed trends  
868 are shown at the top right corner of each plot. Black box denotes the southwestern U.S.  
869 (WST). (b) Time series of fine dust concentration (cyan) and precipitation (purple)  
870 averaged over the WST and their linear trends (dashed lines; values are listed at bottom  
871 left) in spring from 1990 to 2015. Gray shading denotes  $\pm$ one standard error of the  
872 observations. The correlation between fine dust and precipitation is also listed at the  
873 bottom in purple.

874

875 Figure 4. (a) Observed (Obs) and reconstructed (Reg) tends of fine dust concentration ( $\mu\text{g}$   
876  $\text{m}^{-3}$ ) using five factors in summer from 1990-2015. The contributions from each factor  
877 (precipitation, bareness, surface wind, CAPE, and CIN) are also shown (second and third  
878 rows). Dotted areas are significant at the 90% confidence level. Pattern correlation  
879 between reconstructed dust concentration trends and the observed trends are shown at the  
880 right corner of each plot. Black box denotes the central Great Plains (CGP). (b) Time  
881 series of fine dust concentration (cyan), CIN (orange), and CAPE (deep blue) averaged  
882 over the CGP and their linear trends (dashed lines). Gray shading denotes  $\pm$ one standard  
883 error of the observations. (c) Time series of  $T_{700}$ - $T_{dp}$  (black),  $T_{700}$  (green) and  $T_{dp}$  (light  
884 blue) and their linear trends (dashed lines) in summer from 1990 to 2015.

885

886 Figure 5. (a) Time series of fine dust concentration ( $\mu\text{g m}^{-3}$ ) averaged in the CGP (cyan)  
887 and the index of the Great Plains low-level jet (magenta) and their trends (dashed line) in  
888 JJA from 1990 to 2015. Gray shading denotes  $\pm$ one standard error of the observations.  
889 Correlations between the jet index and fine dust concentration, CIN, and near surface  
890 wind speed for (b) 1990-2015 and (c) 2002-2015. Colored circles denotes correlations at  
891 IMPROVE stations, with green outlines denotes the correlation is significant at the 90%  
892 confidence level. Areas significant at the 95% confidence level are dotted in (b) and  
893 significant at the 90% confidence level are dotted in (c).

894

895 Figure 6. Scatter plot of standardized friction velocity ( $U^*$ ) and CIN anomalies for (a) all  
896 days in JJA from 2002-2015, (b) days when fine dust data is available, and (c) dusty days  
897 (when daily fine dust concentration anomaly is greater than one standard deviation).

898

899 Figure 7. Nighttime 532 nm total attenuated backscatter (shading) and depolarization  
900 ratio (black contours, values  $\geq 0.2$  are shown) from CALIOP on August 10<sup>th</sup>, 2007 (top  
901 left) and on June 21<sup>st</sup>, 2013 (bottom left), along with fine dust concentration anomaly ( $\mu\text{g}$   
902  $\text{m}^{-3}$ ; shading, right column) and CIN anomaly (blue contour, only negative values from -  
903 60 to -120  $\text{J kg}^{-1}$  are shown). CALIOP orbit tracks are shown in grey lines (right column)  
904 with cyan part and sampling points (A-F) denote the cross-section shown on the left  
905 column.

906

907 Figure 8. Same as Fig. 10 but for July 2<sup>nd</sup>, 2011 (top) and July 2<sup>nd</sup>, 2012 (bottom). Only  
908 positive CIN anomalies from 25 to 50  $\text{J kg}^{-1}$  are shown (light purple contour).

909 Figure 9. Daily composites of the anomalies of (a) fine dust concentration ( $\mu\text{g m}^{-3}$ ), (b)  
910 CIN ( $\text{J kg}^{-1}$ ), (c) CAPE ( $\text{J kg}^{-1}$ ), (d) 900 hPa wind speed ( $\text{m s}^{-1}$ ), (e) 10 m wind speed ( $\text{m}$   
911  $\text{s}^{-1}$ ), (f)  $U^*$  ( $\text{m s}^{-1}$ ), (g) total precipitation ( $\text{mm day}^{-1}$ ), (h) convective precipitation ( $\text{mm}$   
912  $\text{day}^{-1}$ ), and (i) total cloud cover (%) during dusty days in JJA from 2002 to 2015. Dotted  
913 areas are significant at the 95% confidence level. 900 hPa and 10 m wind anomalies  
914 (green vectors) significant at the 95% confidence level are shown in (d) and (e).

915

916 Figure 10. Daily composite of vertical velocity (shading;  $10^2 \text{ m s}^{-1}$ ), potential  
917 temperature (grey contours; K), and specific humidity (purple contours;  $\text{g kg}^{-1}$ ) from the  
918 ERA-Interim, and fine dust concentration anomalies (bottom; orange line) averaged  
919 between  $95^\circ$  and  $102^\circ$  W for dusty days in JJA from 2002 to 2015. Topography is  
920 masked out in grey. Cyan lines denote the domain of the CGP.

921

922 Figure 11. Daily composites of (a)  $T_{2\text{m}}$  (K) and (b) 850 hPa geopotential height (gpm)  
923 and horizontal wind vectors ( $\text{m s}^{-1}$ ; grey) from the ERA-Interim averaged over dusty days  
924 in JJA from 2002-2015. Blue and red contours denote 1560 geopotential height in the  
925 climatology (2002-2015) and during dusty days, respectively. Areas significant at the  
926 95% confidence level are dotted. Wind vectors significant at the 95% confidence level  
927 are plotted in green.

928

929

930

931

932        Table 1 Correlations between friction velocity ( $U^*$ ) and CIN, CIN and 2 meter  
 933        temperature ( $T_{2m}$ ),  $T_{2m}$  and  $U^*$ ,  $T_{700}-T_{dp}$  (the differences between air temperature at 700  
 934        hPa and 2m dew point temperature) and CIN,  $T_{700}-T_{dp}$  and  $U^*$  for all days in JJA from  
 935        2002 to 2015 (1288 days), days when fine dust concentration is available (431 days), and  
 936        dusty days (52 days). All values are significant at the 95% confidence level (t-test) except  
 937        those listed in italic.

Variables	All days in JJA	Available days	Dusty days
$U^*$ , CIN	-0.54	-0.54	-0.44
CIN, $T_{2m}$	-0.59	-0.59	-0.39
$T_{2m}$ , $U^*$	0.39	0.37	0.19
CIN, $T_{700}-T_{dp}$	-0.59	-0.62	-0.59
$T_{700}-T_{dp}$ , $U^*$	0.37	0.38	0.14

939  
 940  
 941  
 942  
 943        Table 2 Correlations between  $U^*$  and CIN, CIN and vertical wind speed at 850 hPa  
 944        (w850), w850 and  $U^*$  during dusty days in JJA from 2002 to 2015. All values are  
 945        significant at the 95% confidence level except the value significant at the 90% confidence  
 946        level is labeled with a “+” (t-test).

Variables	Dusty days
$U^*$ , CIN	-0.44
CIN, w850	0.28 <sup>+</sup>
w850, $U^*$	-0.32

948  
 949  
 950  
 951  
 952  
 953  
 954  
 955  
 956  
 957  
 958  
 959  
 960  
 961  
 962  
 963  
 964  
 965  
 966  
 967

### Fine dust concentration trend (1990-2015)

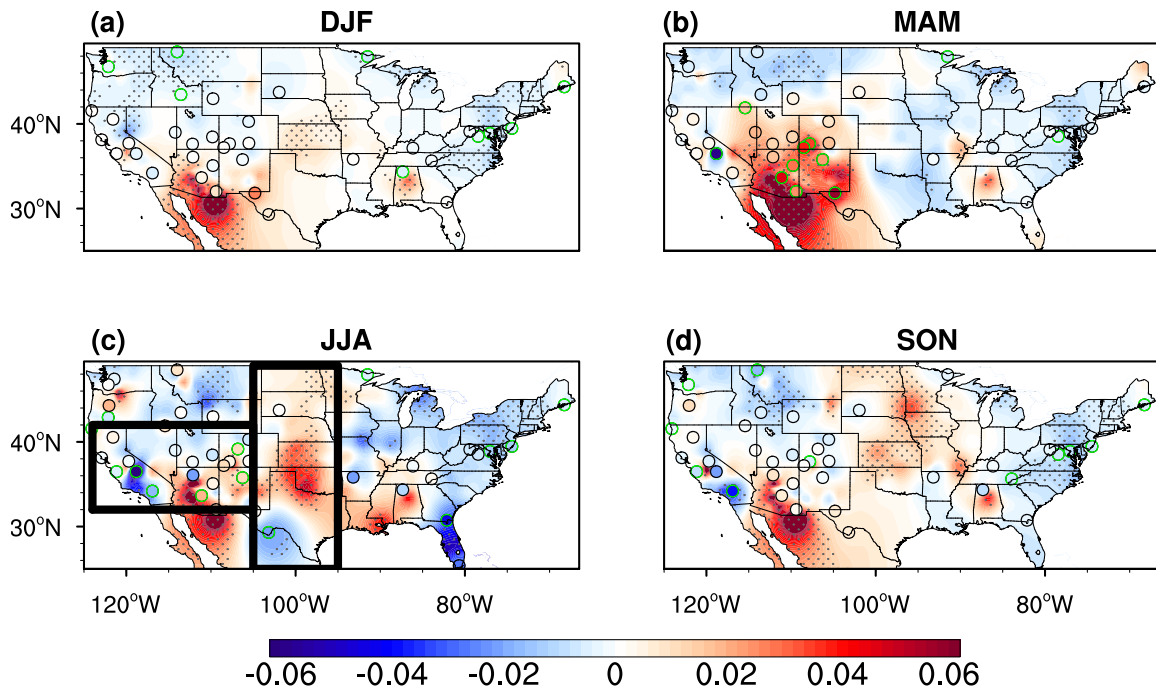
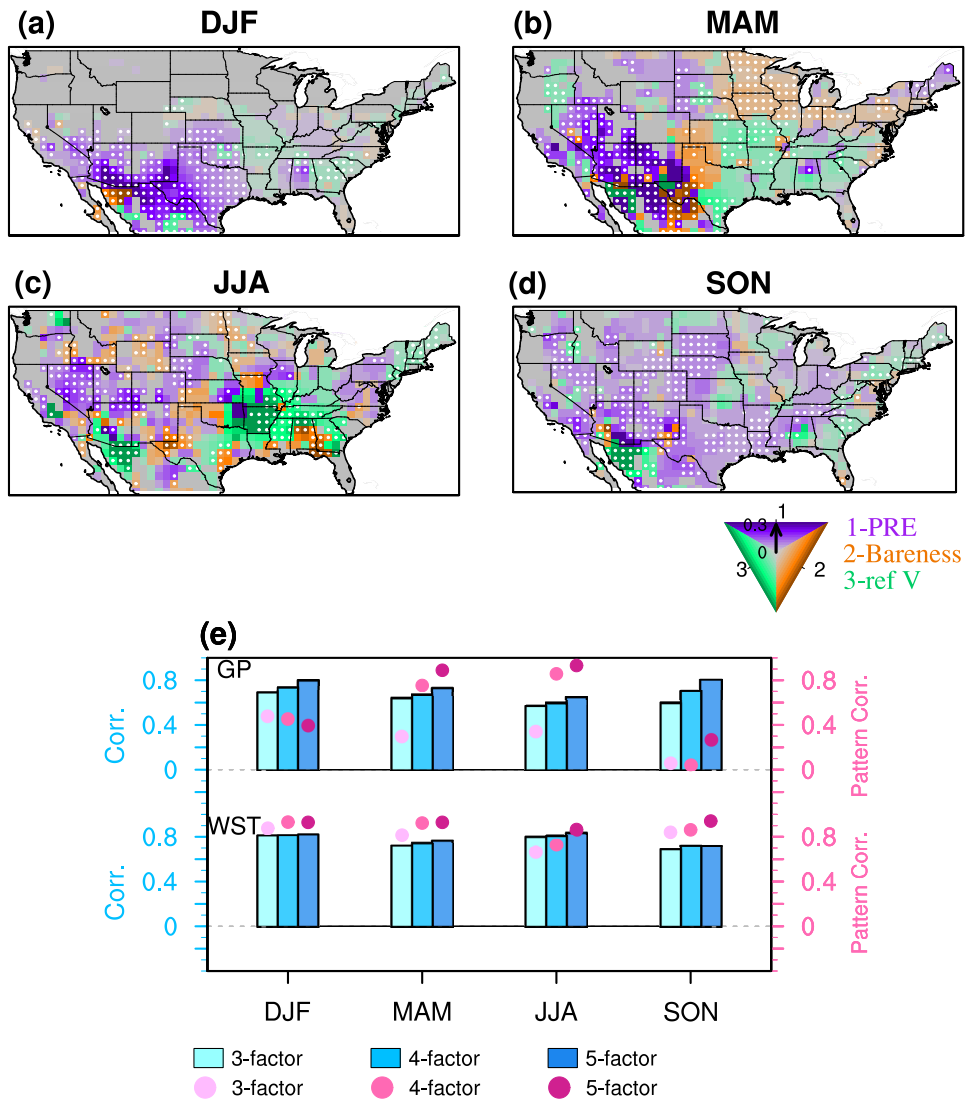


Figure 1. Trend (shading) of fine dust concentration ( $\mu\text{g m}^{-3}$ ) from 1990 to 2015 in (a) DJF, (b) MAM, (c) JJA, and (d) SON from IMPROVE gridded data. Dotted areas are significant at the 95% confidence level. The colored circles show the trend at IMPROVE stations with consecutive records for at least 23 years during 1990-2015. Circles with green outlines denote that the trend is significant at the 90% confidence level. Black boxes denote the averaging areas of the southwestern U.S. (left) and the Great Plains (right).

968  
969  
970  
971  
972  
973  
974  
975  
976  
977  
978  
979  
980  
981

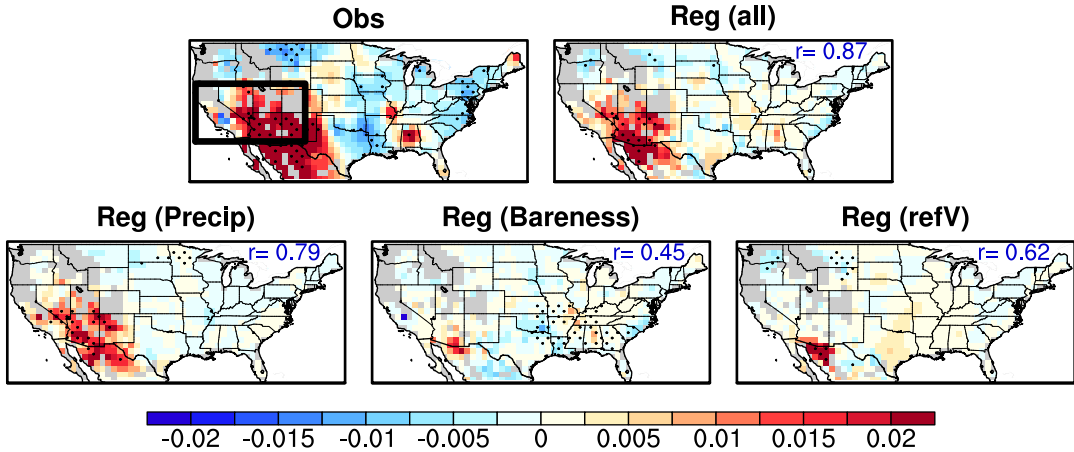


982

983

984 Figure 2. (a)-(d) Multiple linear regression coefficients calculated by regressing fine dust  
 985 concentration from 1990-2015 onto standardized precipitation (purple), bareness  
 986 (orange), and surface wind (green). Color denotes the most influential factor at each grid  
 987 (i.e., the largest regression coefficient in absolute value among the three), while  
 988 saturation of the color shows the magnitude of the coefficient (0 to 0.3). Areas significant  
 989 at the 95% confidence levels are dotted. (e) Bar-plot showing the correlations between  
 990 observed regional mean fine dust concentration and the reconstructed concentration using  
 991 3, 4, and 5 controlling factors (light, median, and deep blue), and pattern correlation  
 992 between trends from the observation and from reconstructed fine dust using 3, 4, and 5  
 993 factors (light, medium, and deep pink) in the Great Plains (GP) and the southwestern U.S.  
 994 (WST, black boxes in Fig. 1). “3-factor” denotes precipitation, bareness, and surface  
 995 wind, “4-factor” denotes precipitation, bareness, surface wind, and CIN, “5-factor”  
 996 denotes precipitation, bareness, surface wind, CIN, and CAPE.  
 997

(a) Obs and Reg fine dust trend (1990-2015 MAM)



(b) WST fine dust and precipitation (MAM)

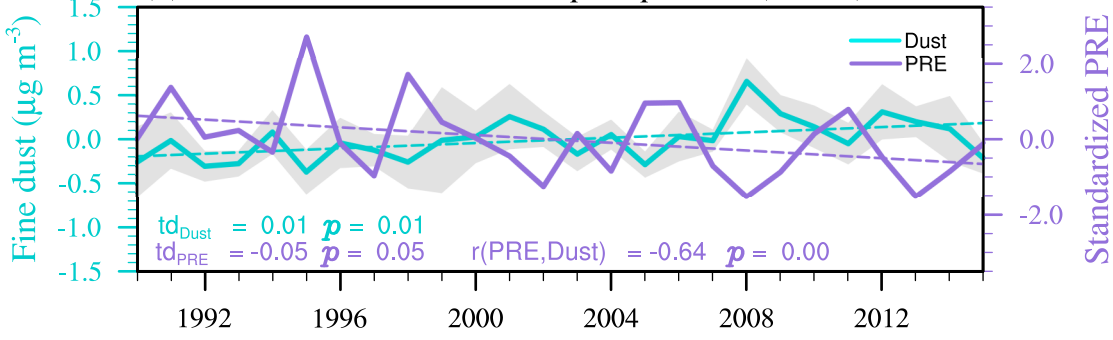


Figure 3. (a) Observed (Obs) and reconstructed (Reg) trends of fine dust concentration ( $\mu\text{g m}^{-3}$ ) using three factors in spring from 1990 to 2015. The contributions from each factor (precipitation, bareness, and surface wind) to the overall reconstructed trend are also shown (second row). Dotted areas are significant at the 90% confidence level. Pattern correlation between reconstructed dust concentration trends and observed trends are shown at the top right corner of each plot. Black box denotes the southwestern U.S. (WST). (b) Time series of fine dust concentration (cyan) and precipitation (purple) averaged over the WST and their linear trends (dashed lines; values are listed at bottom left) in spring from 1990 to 2015. Gray shading denotes  $\pm$ one standard error of the observations. The correlation between fine dust and precipitation is also listed at the bottom in purple.

998  
999  
1000  
1001  
1002  
1003  
1004  
1005  
1006  
1007  
1008  
1009  
1010  
1011  
1012  
1013  
1014  
1015  
1016  
1017

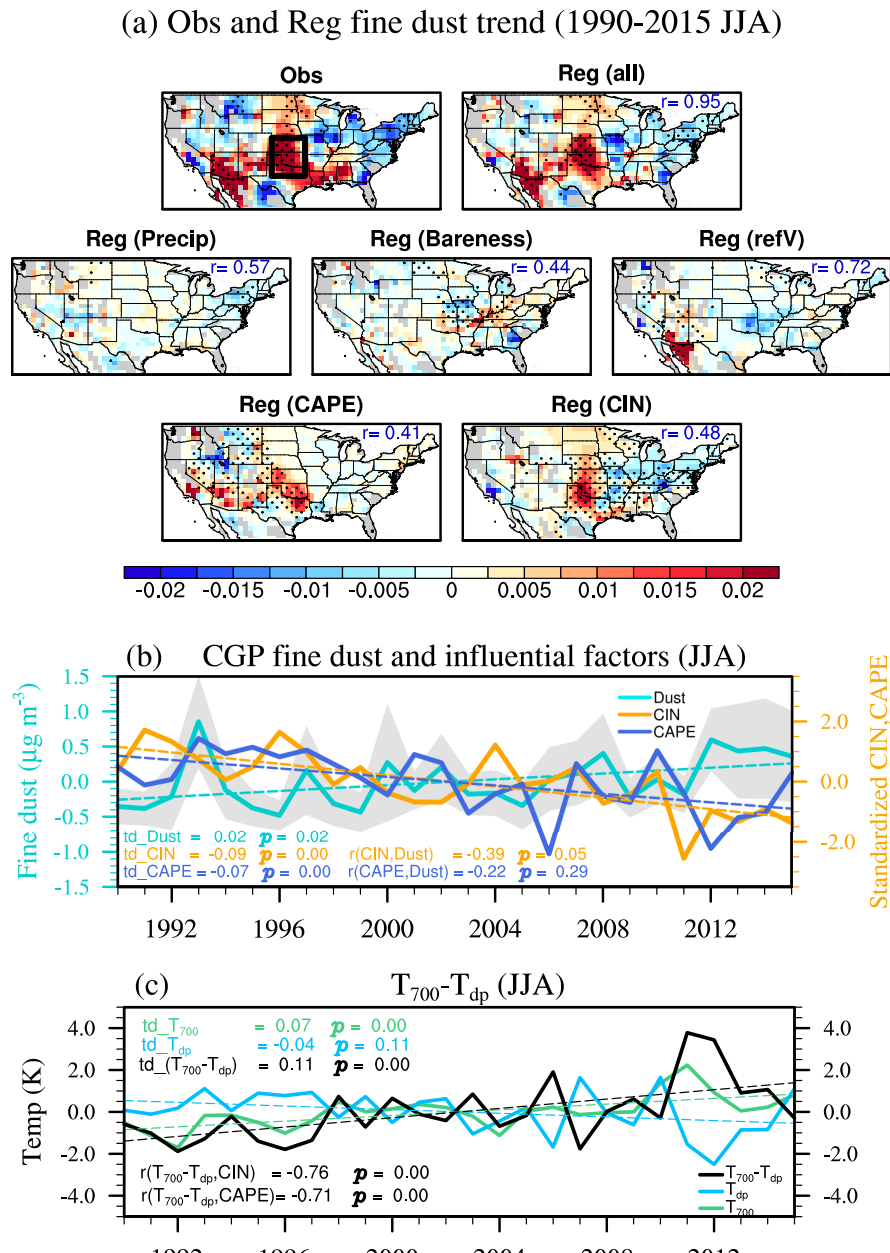
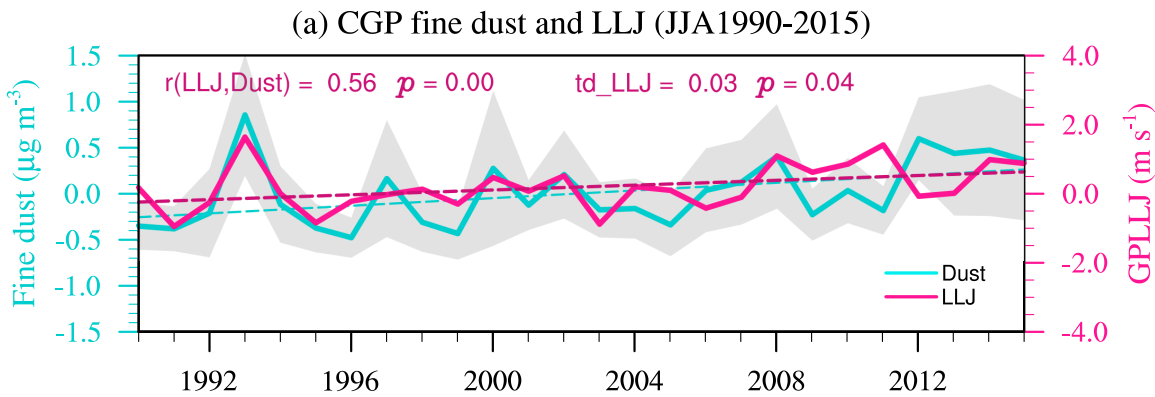
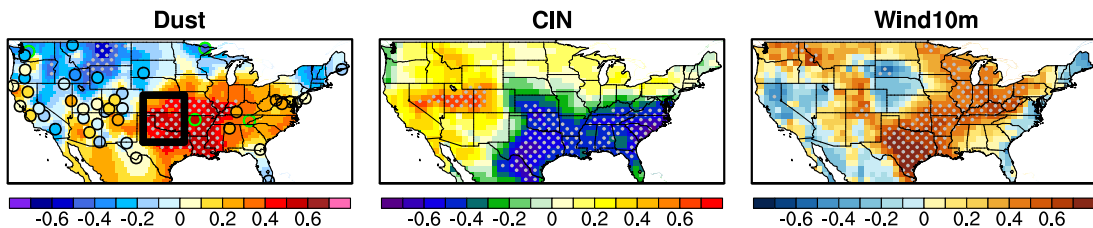


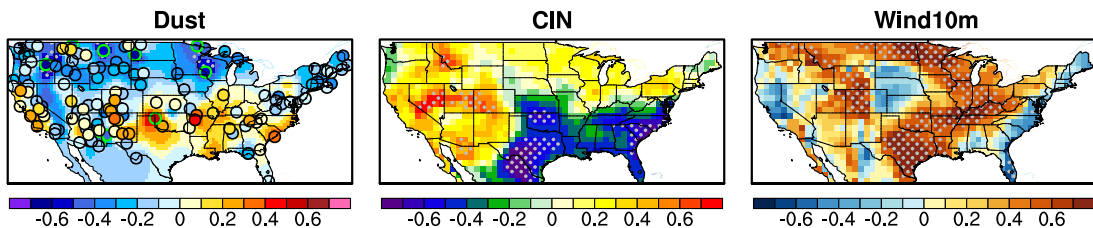
Figure 4. (a) Observed (Obs) and reconstructed (Reg) trends of fine dust concentration ( $\mu\text{g m}^{-3}$ ) using five factors in summer from 1990-2015. The contributions from each factor (precipitation, bareness, surface wind, CAPE, and CIN) are also shown (second and third rows). Dotted areas are significant at the 90% confidence level. Pattern correlation between reconstructed dust concentration trends and the observed trends are shown at the right corner of each plot. Black box denotes the central Great Plains (CGP). (b) Time series of fine dust concentration (cyan), CIN (orange), and CAPE (deep blue) averaged over the CGP and their linear trends (dashed lines). Gray shading denotes  $\pm$  one standard error of the observations. (c) Time series of  $T_{700} - T_{dp}$  (black),  $T_{700}$  (green) and  $T_{dp}$  (light blue) and their linear trends (dashed lines) in summer from 1990 to 2015.



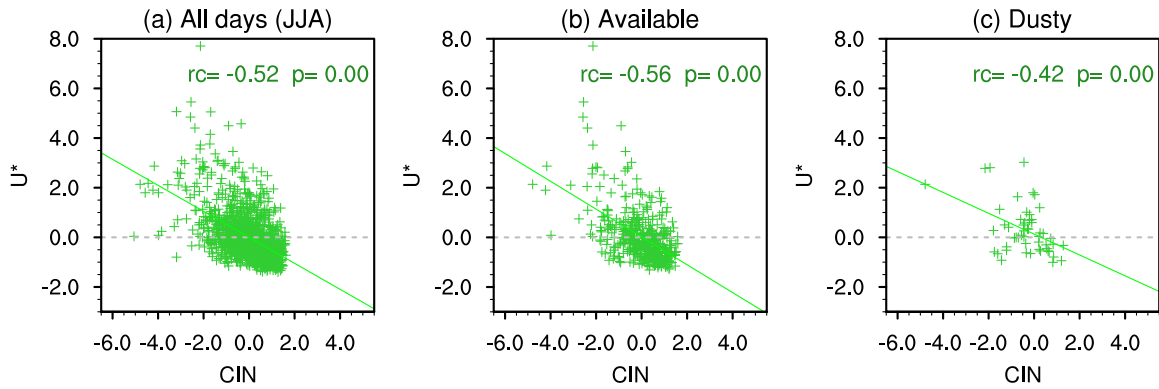
(b) Correlation with the LLJ (1990-2015)



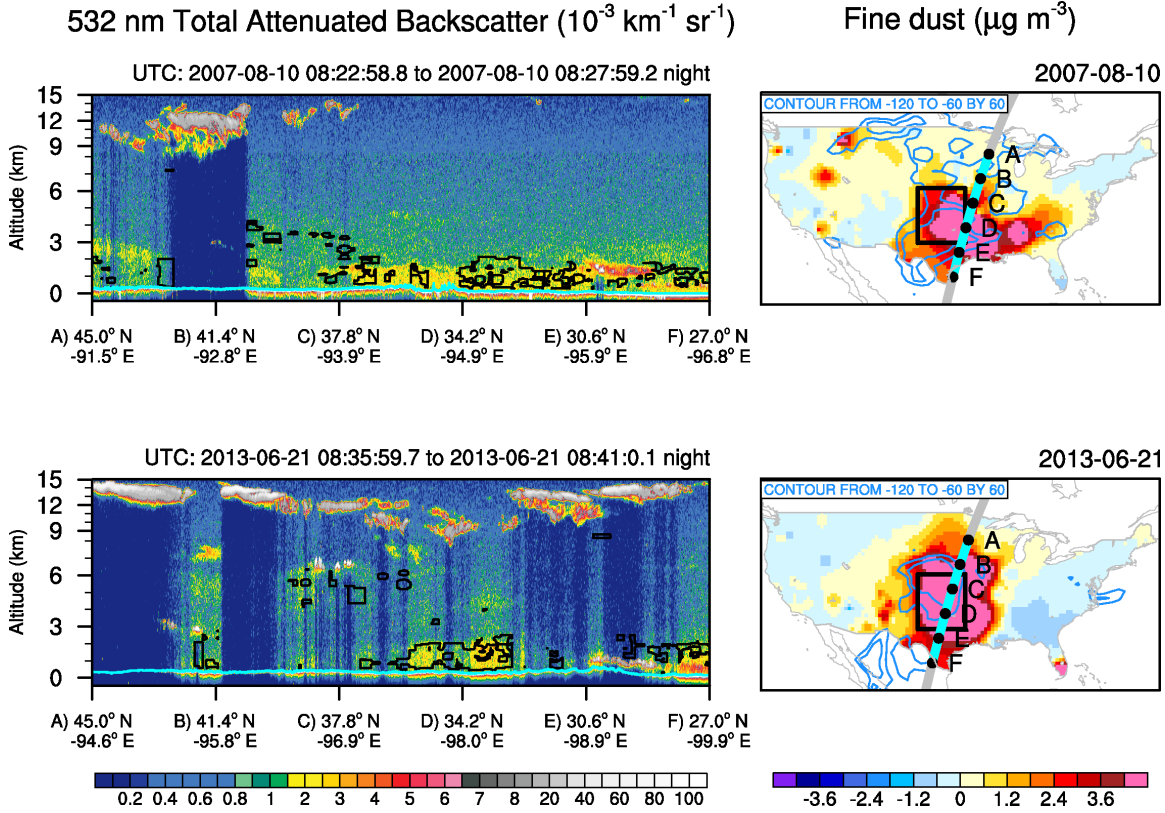
(c) Correlation with the LLJ (2002-2015)



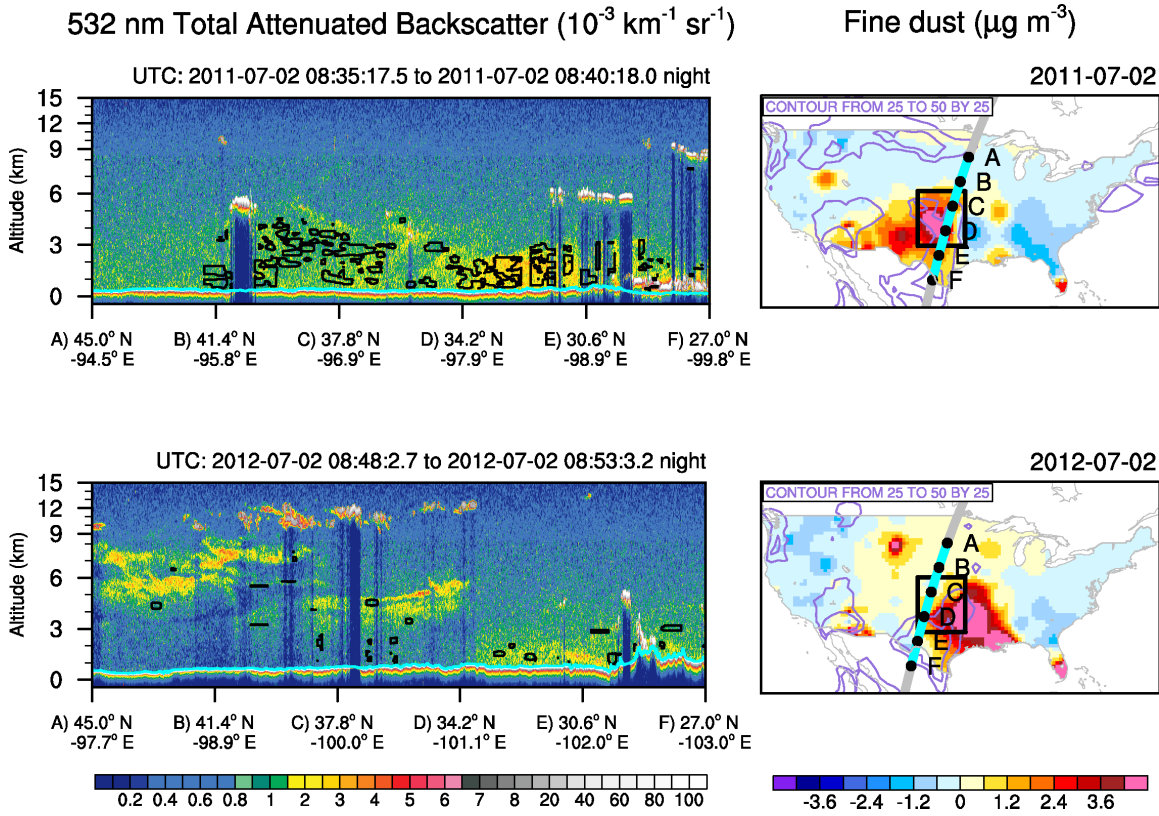
1030  
1031 Figure 5. (a) Time series of fine dust concentration ( $\mu\text{g m}^{-3}$ ) averaged in the CGP (cyan)  
1032 and the index of the Great Plains low-level jet (magenta) and their trends (dashed line) in  
1033 JJA from 1990 to 2015. Gray shading denotes  $\pm$ one standard error of the observations.  
1034 Correlations between the jet index and fine dust concentration, CIN, and near surface  
1035 wind speed for (b) 1990-2015 and (c) 2002-2015. Colored circles denotes correlations at  
1036 IMPROVE stations, with green outlines denotes the correlation is significant at the 90%  
1037 confidence level. Areas significant at the 95% confidence level are dotted in (b) and  
1038 significant at the 90% confidence level are dotted in (c).  
1039  
1040  
1041  
1042  
1043  
1044  
1045  
1046



1047  
1048 Figure 6. Scatter plot of standardized friction velocity ( $U^*$ ) and CIN anomalies for (a) all  
1049 days in JJA from 2002-2015, (b) days when fine dust data is available, and (c) dusty days  
1050 (when daily fine dust concentration anomaly is greater than one standard deviation).  
1051  
1052  
1053  
1054  
1055  
1056  
1057  
1058  
1059  
1060  
1061  
1062  
1063  
1064  
1065  
1066  
1067  
1068  
1069  
1070  
1071  
1072  
1073  
1074  
1075  
1076  
1077  
1078  
1079  
1080

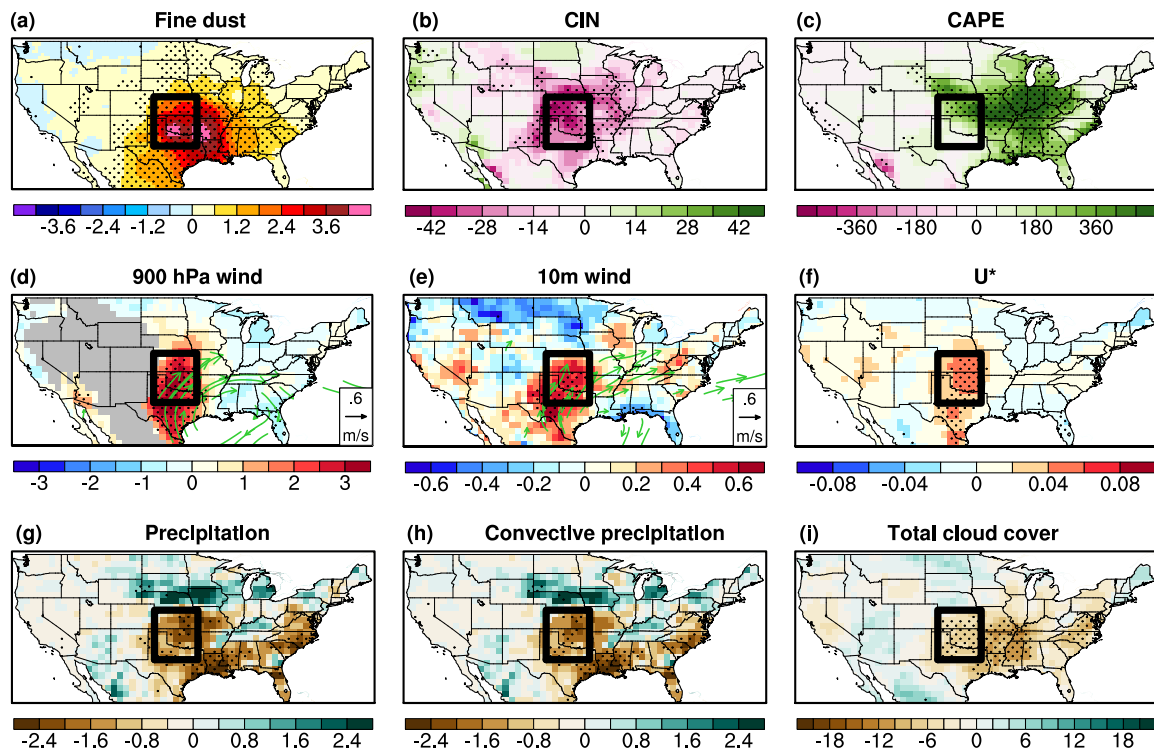


1081  
1082 Figure 7. Nighttime 532 nm total attenuated backscatter (shading)  
1083 and depolarization ratio (black contours, values  $\geq 0.2$  are shown) from CALIOP on August 10<sup>th</sup>, 2007 (top  
1084 left) and on June 21<sup>st</sup>, 2013 (bottom left), along with fine dust concentration anomaly ( $\mu\text{g}$   
1085  $\text{m}^{-3}$ ; shading, right column) and CIN anomaly (blue contour, only negative values from -  
1086 60 to -120  $\text{J kg}^{-1}$  are shown). CALIOP orbit tracks are shown in grey lines (right column)  
1087 with cyan part and sampling points (A-F) denote the cross-section shown on the left  
1088 column.  
1089  
1090  
1091  
1092  
1093  
1094  
1095  
1096  
1097  
1098  
1099  
1100  
1101  
1102  
1103  
1104  
1105



1106  
1107 Figure 8. Same as Fig. 10 but for July 2<sup>nd</sup>, 2011 (top) and July 2<sup>nd</sup>, 2012 (bottom). Only  
1108 positive CIN anomalies from  $25 \text{ to } 50 \text{ J kg}^{-1}$  are shown (light purple contour).  
1109  
1110  
1111  
1112  
1113  
1114  
1115  
1116  
1117  
1118  
1119  
1120  
1121  
1122  
1123  
1124  
1125  
1126  
1127  
1128  
1129

### Daily composite (among JJA0215)



1130 Figure 9. Daily composites of the anomalies of (a) fine dust concentration ( $\mu\text{g m}^{-3}$ ), (b)  
 1131 CIN ( $\text{J kg}^{-1}$ ), (c) CAPE ( $\text{J kg}^{-1}$ ), (d) 900 hPa wind speed ( $\text{m s}^{-1}$ ), (e) 10 m wind speed ( $\text{m}$   
 1132  $\text{s}^{-1}$ ), (f)  $U^*$  ( $\text{m s}^{-1}$ ), (g) total precipitation ( $\text{mm day}^{-1}$ ), (h) convective precipitation ( $\text{mm}$   
 1133  $\text{day}^{-1}$ ), and (i) total cloud cover (%) during dusty days in JJA from 2002 to 2015. Dotted  
 1134 areas are significant at the 95% confidence level. 900 hPa and 10 m wind anomalies  
 1135 (green vectors) significant at the 95% confidence level are shown in (d) and (e).

1136

1137

1138

1139

1140

1141

1142

1143

1144

1145

1146

1147

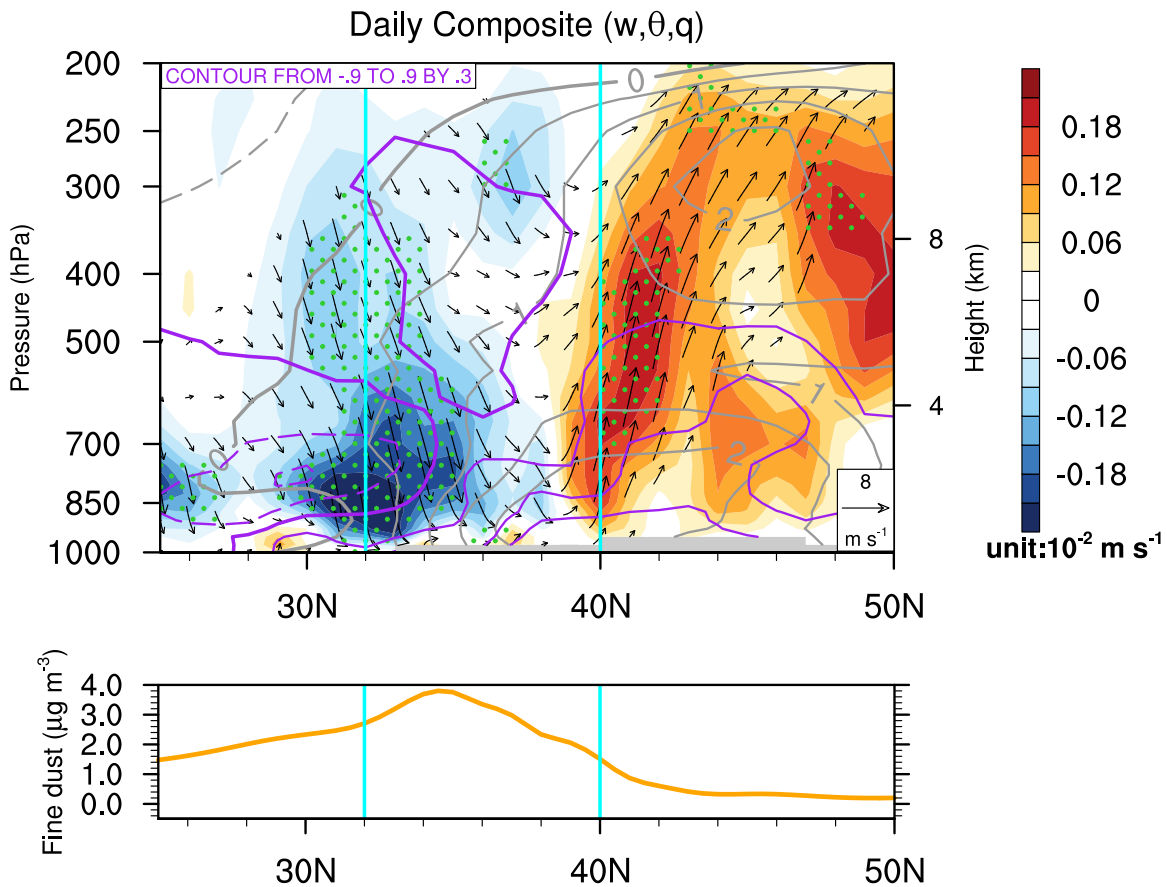
1148

1149

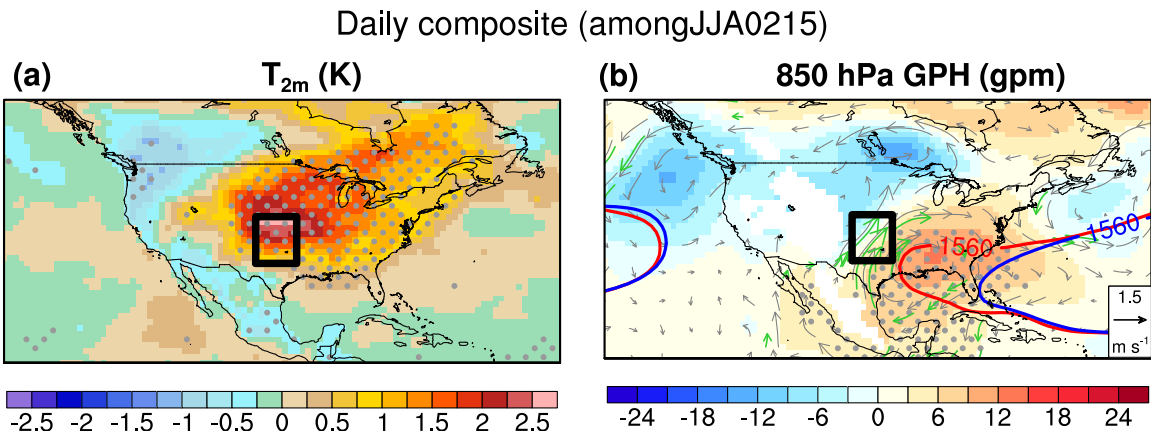
1150

1151

1152



1153  
1154 Figure 10. Daily composite of vertical velocity (shading;  $10^{-2} \text{ m s}^{-1}$ ), potential  
1155 temperature (grey contours; K), and specific humidity (purple contours;  $\text{g kg}^{-1}$ ) from the  
1156 ERA-Interim, and fine dust concentration anomalies (bottom; orange line) averaged  
1157 between  $95^\circ$  and  $102^\circ$  W for dusty days in JJA from 2002 to 2015. Topography is  
1158 masked out in grey. Cyan lines denote the domain of the CGP.  
1159  
1160  
1161  
1162  
1163  
1164  
1165  
1166  
1167  
1168  
1169  
1170  
1171  
1172  
1173  
1174  
1175



1176  
 1177  
 1178  
 1179  
 1180  
 1181  
 1182  
 1183

Figure 11. Daily composites of (a)  $T_{2m}$  (K) and (b) 850 hPa geopotential height (gpm) and horizontal wind vectors ( $m s^{-1}$ ; grey) from the ERA-Interim averaged over dusty days in JJA from 2002-2015. Blue and red contours denote 1560 geopotential height in the climatology (2002-2015) and during dusty days, respectively. Areas significant at the 95% confidence level are dotted. Wind vectors significant at the 95% confidence level are plotted in green.